



UNIVERSITY OF LEEDS

This is a repository copy of *Evaluation of (15)N-detected H-N correlation experiments on increasingly large RNAs.*

White Rose Research Online URL for this paper:
<http://eprints.whiterose.ac.uk/122778/>

Version: Accepted Version

Article:

Schnieders, R, Richter, C, Warhaut, S et al. (10 more authors) (2017) Evaluation of (15)N-detected H-N correlation experiments on increasingly large RNAs. *Journal of Biomolecular NMR*, 69 (1). pp. 31-44. ISSN 1573-5001

<https://doi.org/10.1007/s10858-017-0132-7>

© 2017, Springer. This is an author produced version of a paper published in *Journal of Biomolecular NMR*. Uploaded in accordance with the publisher's self-archiving policy. The final publication is available at <http://dx.doi.org/10.1007/s10858-017-0132-7>

Reuse

Items deposited in White Rose Research Online are protected by copyright, with all rights reserved unless indicated otherwise. They may be downloaded and/or printed for private study, or other acts as permitted by national copyright laws. The publisher or other rights holders may allow further reproduction and re-use of the full text version. This is indicated by the licence information on the White Rose Research Online record for the item.

Takedown

If you consider content in White Rose Research Online to be in breach of UK law, please notify us by emailing eprints@whiterose.ac.uk including the URL of the record and the reason for the withdrawal request.



eprints@whiterose.ac.uk
<https://eprints.whiterose.ac.uk/>

Evaluation of ¹⁵N-detected H-N correlation experiments on increasingly large RNAs

Robbin Schnieders¹, Christian Richter¹, Sven Warhaut¹, Vanessa de Jesus¹, Sara Keyhani¹, Elke Duchardt-Ferner², Heiko Keller², Jens Wöhnert², Lars T. Kuhn³, Alexander L. Breeze³, Wolfgang Bermel⁴, Harald Schwalbe^{1,*}, Boris Fürtig^{1,*}

*correspondence to Prof. Dr. Harald Schwalbe – schwalbe@nmr.uni-frankfurt.de, 069 798 29737 or to Dr. Boris Fürtig – fuertig@nmr.uni-frankfurt.de, 069 798 29157

¹Institute for Organic Chemistry and Chemical Biology
Center for Biomolecular Magnetic Resonance (BMRZ)
Johann Wolfgang Goethe-Universität Frankfurt
Max-von-Laue-Str. 7
D-60438 Frankfurt

²Institute for Molecular Biosciences
Center for Biomolecular Magnetic Resonance (BMRZ)
Johann Wolfgang Goethe-Universität Frankfurt
Max-von-Laue Str. 9
D-60438 Frankfurt

³Astbury Centre for Structural Molecular Biology,
Faculty of Biological Sciences
University of Leeds
Leeds LS2 9JT, UK

⁴Bruker BioSpin GmbH
Silberstreifen 4
D-76287 Rheinstetten

Keywords

¹⁵N direct detection, RNA, BEST-TROSY, line width analysis, field dependence, exchange

Abstract

Recently, ^{15}N -detected multidimensional NMR experiments have been introduced for the investigation of proteins. Utilization of the slow transverse relaxation of nitrogen nuclei in a ^{15}N -TROSY experiment allowed recording of high quality spectra for high molecular weight proteins, even in the absence of deuteration.

Here, we demonstrate the applicability of three ^{15}N -detected H-N correlation experiments (TROSY, BEST-TROSY and HSQC) to RNA. With the newly established ^{15}N -detected BEST-TROSY experiment, which proves to be the most sensitive ^{15}N -detected H-N correlation experiment, spectra for five RNA molecules ranging in size from 5 kDa to 100 kDa were recorded. These spectra yielded high resolution in the ^{15}N -dimension even for larger RNAs since the increase in line width with molecular weight is more pronounced in the ^1H - than in the ^{15}N -dimension. Further, we could experimentally validate the difference in relaxation behavior of imino groups in AU and GC base pairs. Additionally, we showed that ^{15}N -detected experiments theoretically should benefit from sensitivity and resolution advantages at higher static fields but that the latter is obscured by exchange dynamics within the RNAs.

Introduction

Recently, the direct detection of heteronuclei in NMR spectroscopy of proteins¹ experienced a renaissance², mainly due to significant improvements in cryogenic probes and the availability of high magnetic fields. These advances have made low- γ nuclei detection schemes feasible even at relatively low sample concentrations of around 0.5 mM^{3,4}. Furthermore, the size of proteins under study is constantly increasing. This causes two major difficulties: resonance overlap and line broadening. Line broadening is not only mediated by the mere size of the molecule but also by the exchange of two or more conformational states as well as by base catalyzed solvent exchange.

These problems are less severe for heteronuclei. Compared to protons, carbon- and nitrogen-nuclei exhibit a wider frequency dispersion and a slower decay of signals due to intrinsically smaller transverse relaxation rates². In addition, solvent exchange does not directly affect the signals, even under unfavorable conditions such as physiological temperature and pH⁵.

The initial heteronuclei-detected NMR experiments for proteins focused on ¹³C direct-detection^{6,7} and were followed by direct-detected ¹⁵N NMR experiments⁸⁻¹⁰. Particularly, the ¹⁵N-detected CAN and CON experiments⁹ as well as the hCAN experiment¹⁰ have proven their value in high resolution spectra. Despite the lower gyromagnetic ratio, the CAN and CON experiments show a sensitivity comparable to their ¹³C-detected counterparts⁹. The hCAN experiment further increases sensitivity by ¹H-excitation which goes along with shorter proton longitudinal relaxation time and therefore offers the possibility for shorter inter-scan delays¹⁰.

Recently, it was shown that under certain experimental conditions the ¹⁵N-detected TROSY-HSQC experiment applied to proteins is nearly as sensitive as its proton detected analogue^{11,12}: First, the experiment is performed on a large protein (MW > 42 kDa) since transverse relaxation rates increase faster for ¹H- than for ¹⁵N-nuclei with molecular size. Second, the protein under investigation is non-deuterated which increases ¹H transverse relaxation rates by another factor of three, whereas ¹⁵N relaxation rates stay unperturbed. This reduces sample cost and permits NMR studies of proteins that cannot be expressed in *E. coli*. Third, salt concentrations are increased to at least 200 mM NaCl mimicking *in vivo* conditions which reduces ¹H-sensitivity by approximately 50% but ¹⁵N-sensitivity only about 5%.

For nucleic acids, an analog suite of ¹³C-detected experiments has been developed to correlate resonances within the sugar-phosphate backbone or within the nucleobase¹³⁻¹⁵. Due to the small proton chemical shift dispersion in nucleic acids and the low proton density in this class of biomolecules these experiments are beneficial. Further, they do not depend on the detection of the exchangeable imino proton resonances which are only visible in stable secondary structures. ¹³C-detected NMR experiments are often less sensitive than ¹H-detected experiments but they provide additional information about rather flexible regions of RNA¹⁶.

Even though having a diverse set of NMR experiments at hand, with few exceptions¹⁷ the current molecular size limit in investigation of RNA molecules is at approximately 150 nt using site specific labeling schemes¹⁸. However, the desired target size of biologically relevant RNA, e.g. long non-coding RNAs, often exceeds

250 nt¹⁹. The necessity to overcome the size limitation of the RNA under study prompted us to analyze the applicability of not only ¹³C but also ¹⁵N direct-detected NMR experiments to RNAs. So far, only one-dimensional ¹⁵N-detected experiments have been used to study RNAs²⁰⁻²². For site-selective ¹⁵N-labelled sequences chemical shift differences upon addition of metal ions allowed the mapping of binding sites²⁰.

We here apply ¹⁵N-detected HSQC¹⁵ and TROSY¹⁰ experiments to RNA and develop an improved ¹⁵N-detected BEST-TROSY. For the ¹⁵N-detected BEST-TROSY experiment, we demonstrate application to five RNAs ranging in size from 14 nt to 329 nt and investigate the effect of molecular size on resolution, sensitivity and relaxation behavior in comparison to the ¹H-detected BEST-TROSY experiment. As expected, we observe a significantly faster increase in line width with molecular size for the signals in the ¹H-dimensions. Further, we analyze the effect of base pair type, chemical exchange and conformational equilibria on ¹⁵N and ¹H signal line widths. We can show that imino protons in AU base pairs exhibit smaller line widths compared to GC base pairs in both, the ¹H- and the ¹⁵N-dimension. Additionally, we show that resolution does not improve when measuring at 950 MHz (22.3 T) in comparison to 800 MHz (18.8 T) spectrometers whereas sensitivity is increased as expected according to the higher field strength.

Materials and methods

14 nt RNA

The uniformly ^{13}C - ^{15}N -labeled 14 nt RNA containing a cUUCGg tetraloop (5'-pppGGCACUUCGGUGCC-3') was prepared via *in vitro* transcription and purchased from Silantes (Munich, Germany). The 400 μM NMR sample was dissolved in NMR buffer (25 mM potassium phosphate, pH 6.4) containing 10% D_2O . The assignment of the imino protons was taken from the previously published resonance assignment (BMRB-entry 5705)²⁴.

40 nt RNA

The ^{13}C - ^{15}N -uridine labeled 40 nt RNA represents the expression platform of the 2'-dG sensing riboswitch of *Mesoplasma fluorum* (5'-pppGGAAAGUUUCUUUUUAUGUCCAAAAGACAGAAAGAAACUU-3'). This RNA was prepared from a PCR-amplified DNA fragment via *in vitro* transcription with T7 RNA polymerase as described¹⁶. The following description will therefore only contain deviations from this protocol. For PCR amplification, a concentration of 0.5 μM of each primer was used. The transcription was performed under the following conditions: 100 mM Tris-glutamic acid (pH 8.1), 2 mM spermidine, 20 mM dithiothreitol (DTT), 2% (v/v) PCR mixture, 15 mM $\text{Mg}(\text{OAc})_2$, 7 mM of each rNTP, 20% (v/v) DMSO, 0.2 U/mL yeast inorganic pyrophosphatase (YIPP, NEB) and 144 nM T7 RNA polymerase²⁵. The NMR sample was further purified using the published buffer exchange protocol²⁶ and was transferred into NMR buffer (25 mM potassium phosphate, pH 6.2) containing 8% D_2O . The final RNA concentration was 2 mM.

47 nt RNA

^{13}C - ^{15}N -uridine labeled RNA encoding the 47 nt fluoride riboswitch from *Bacillus cereus*²⁷ (5'-pppGGCGAUGGUGUUCGCCAUAAACGCUCUUCGGAGCUAAUGACACCUAC-3') followed by a self-splicing HDV ribozyme²⁸ was prepared by run-off *in vitro* transcription from linearized plasmid DNA using T7 RNA polymerase as described²⁹. Co-transcriptional ribozyme self-cleavage released the *Bacillus cereus* fluoride riboswitch RNA and ensured RNA 3' end homogeneity. ^{13}C - ^{15}N -labeled rUTP was purchased from Silantes (Munich, Germany).

The RNA was folded in the presence of 50 mM potassium acetate (pH 6.1) by denaturing at 95°C for 10 minutes and subsequent annealing on ice for 30 minutes. The folded RNA was incubated with 2.5 mM EDTA for 10 minutes at room temperature to complex residual Mg^{2+} ions. The RNA was transferred into NMR buffer (50 mM potassium acetate, pH 6.1) while stepwise diluting the EDTA to a concentration below 100 nM. The NMR sample of the 47 nt RNA contained 1 mM RNA, 10 mM magnesium acetate and 7.5% D_2O in 50 mM potassium acetate (pH 6.1). The resonance assignment of uridine imino protons was deduced from ^1H , ^1H -NOESY, ^{15}N -HSQC, H(N)CO and HNN-COSY spectra (unpublished data).

74 nt RNA

The 74 nt Spinach RNA (5'-pppGGGACCGAAAUGGUGAAGGACGGGUCCAGUGCUUCGGCAGUGUUGAGUAGAGUGUGAGCUCCGUAACUGGUCCC-3'), which forms a stable complex with the fluorogenic ligand 3,5-dihydro-4-fluorobenzylidene-imidazolinone (DFHBI) featuring an internal RNA G-quadruplex³⁰, was synthesized with T7 RNA polymerase by *in vitro* transcription from with Smal (New England Biolabs) linearized plasmid and purified by preparative polyacrylamide gel electrophoresis as described³¹. ¹⁵N-labeled rUTP and rGTP were used (Silantes, Germany), all other rNTPs were purchased from Carl Roth GmbH (Karlsruhe, Germany). DFHBI was obtained commercially from Lucerna Inc. After purification, the RNA was folded by snap cooling in 5 volumes ice cold water after heating to 95 °C for 5 min. The RNA was transferred into HEPES buffer. The final concentration of the NMR sample was 200 μM and it contained 5 mM DFHBI, 40 mM HEPES and 125 mM KCl in 8% D₂O at a pH value of 7.5. NH-resonance assignment was inferred from ¹H, ¹H-NOESY and ¹⁵N-HSQC data (unpublished data).

127 nt RNA

The adenine-sensing full length riboswitch, consisting of 127 nt (5'-GCUUCAUUAUAUCCUAAUGAUAUGGUUUGGGAGUUUCUACCAAGAGCCUUAACUCUUGAUUAUGAAGUCUGUCGCUUUAUCCGAAAUUUUAUAAAGAGAAGACUCAUGAAUUACUUUGACCUGCCG-3'), from *Vibrio vulnificus*³² was synthesized from a PCR amplified DNA template via *in vitro* transcription with T7 RNA polymerase as described²⁶. For 5' homogeneity of the construct, a 5'-hammerhead ribozyme was used. The construct was purified using a DEAE column as described³³ and preparative polyacrylamide gel electrophoresis according to standard protocols. The ¹⁵N-labeled nucleotides for transcription (rGTP and rUTP) were purchased from Silantes (Munich, Germany) whereas all other rNTPs were purchased from Carl Roth GmbH (Karlsruhe, Germany). The construct was folded in water for 5 min at 95°C at a concentration of 0.3 mM and was immediately diluted 10-fold with ice-cold water. The RNA was buffer-exchanged into NMR buffer (25 mM potassium phosphate, 50 mM KCl, pH 6.2), and supplemented with 5 mM Mg²⁺, 10% D₂O as well as 100 μM DSS. The final concentration was 500 μM. This riboswitch was analyzed in absence and presence of 1.4 eq ¹³C-¹⁵N-labeled adenine. ¹³C-¹⁵N-labeled adenine was synthesized as described³⁴.

329 nt RNA

The ¹³C-¹⁵N-labeled 329 nt long RNA construct was prepared via *in vitro* transcription from linearized plasmid as described³⁵. It consists of 97 CUG triplets and includes a 5' (GGGAGACCGGCAGAUUCUGAUUAUCAUCAUGAAUU) and a 3' overhang (GGGG). The RNA was purified as described³⁶. For refolding of the construct a previously published protocol was used³⁵. The RNA was transferred into NMR buffer (25 mM potassium phosphate, 50 mM potassium chloride, pH 6.4) containing 8% D₂O and having a final concentration of 700 μM.

NMR spectroscopy

All ¹⁵N-detected NMR experiments were carried out on an 800 MHz Bruker NMR spectrometer (18.8 T) equipped with a 5 mm, z-axis gradient ¹³C, ¹⁵N [¹H]-TXO cryogenic probe (¹³C, ¹⁵N on the inner coil and ¹H

on the outer, ^{13}C optimized). Using this probe, the sensitivity for low-gamma nuclei increases by factors of 2 or more in comparison to the respective sensitivity for low-gamma nuclei on a TCI probe. Reasons for this sensitivity increase are a higher filling factor and cold preamplifiers for both nuclei. All ^1H -detected NMR experiments were conducted on an 800 MHz Bruker NMR spectrometer (18.8 T) equipped with a 5 mm, z-axis gradient ^1H [^{13}C , ^{15}N]-TCI cryogenic probe (^1H on the inner coil and ^{13}C , ^{15}N on the outer, without cold ^{15}N preamplifier). This change of spectrometer was necessary for reasons of comparison, since the probes are similarly optimized for the respective nucleus. The ^{15}N -detected BEST-TROSY experiments of the 14 nt, 127 nt and 329 nt RNAs were additionally performed on a 950 MHz Bruker NMR spectrometer (22.3 T) equipped with a 5 mm, z-axis gradient ^{13}C , ^{15}N [^1H]-TXO cryogenic probe (^{15}N optimized). All experiments were carried out at 298 K. Recording of ^{15}N -detected HSQCs was achieved using a standard pulse sequence³⁷ with additional ^{13}C -decoupling during acquisition. For the ^{15}N -detected TROSY-experiment, we applied a pulse sequence published earlier for application to protein¹¹. The ^{15}N -detected BEST-TROSY was performed with a newly established pulse sequence (Fig 1) which is described in the text. For the ^1H -detected reference BEST-TROSY experiments, the standard pulse sequence was used (Topspin 3.5 pl6)^{38,39}. The ω_1 - and ω_2 -axis of the ^{15}N -detected experiments were transposed in the Figures for better comparison with the ^1H -detected equivalents. Signal-to-noise (S/N) ratios were determined from 1D rows of the 2D spectra using the standard "sino" function (Topspin 3.5 pl6). The highest occurring value of the signal region is divided by the RMSD of the noise region. Line widths were determined by processing the spectra without a filter function in the respective direct dimension so that the maximal achievable resolution is not biased.

Results and discussion

Application of different ^{15}N -detected experiments

In this work, we conduct ^{15}N -detected H-N correlation experiments to test their applicability for studying RNA molecules of various size and dynamic properties. At first, we test different ^{15}N -detected pulsing schemes on a well-characterized 14 nt hairpin RNA⁴⁰.

We intend to utilize the slow relaxation properties of the ^{15}N -nucleus that should always exhibit longer T_2 times than the ^1H -nucleus in the slow tumbling limit, according to Redfield theory⁴¹. To optimally sample the FID in the respective experiments, we determine T_2 times for $^1\text{H}^{\text{N}}$ and $^{15}\text{N}^{\text{H}}$ using Carr-Purcell-Meiboom-Gill (CPMG) experiments. The $^{15}\text{N}^{\text{H}}$ T_2 times are in the range of 0.17 s (G9) to 0.29 s (G12).

The spread of the effective $^1\text{H}^{\text{N}}$ T_2 over all imino protons is typically large in RNAs. In the 14 nt hairpin RNA they range between 0.02 s (G9) and 0.10 s (G12). If measured using pulse-sequences containing a CPMG element that partly quenches the imino proton exchange, the $^1\text{H}^{\text{N}}$ T_2 times represent an upper limit of the effective T_2 . Nevertheless, for imino protons involved in stable Watson-Crick base pairs the spin-echo- and CPMG-derived relaxation constants are similar (e.g. $T_2^{\text{SE}} = 0.075$ s and $T_2^{\text{CPMG}} = 0.066$ s for residue G2).

Based on these T_2 times, the optimal acquisition times would sample the FID for at least $3 \cdot T_2$, which results in $aq_{\text{opt}}(^{15}\text{N}) \sim 0.9$ s and $aq_{\text{opt}}(^1\text{H}) \sim 0.3$ s. Since ^{13}C -decoupling must be applied in ^{15}N -detected experiments in double labelled samples, the acquisition time in the direct dimension must be limited to a maximum of 0.3 s (corresponding here to $1 \cdot T_2$) to prevent sample heating.

According to Rovnyak *et al.*⁴², the maximum S/N ratio is reached at an acquisition time of $1.26 \cdot T_2$ in the indirect dimension. In turn, this reduces the achievable resolution but otherwise the S/N ratio per sampled FID would decrease at longer evolution times.

Ultimately, recording the ^{15}N -detected experiments with acquisition times of 0.3 s in the direct ^{15}N - and 0.126 s in the indirect ^1H -dimension will result in the best S/N ratio and achieve the maximum resolution in the ^{15}N -dimension that is technically achievable.

These settings are used in the comparison of the different ^{15}N -detected H-N correlation experiments, namely the ^{15}N -detected HSQC, TROSY and BEST-TROSY experiment. The latter experiment represents a modification of the previously published ^{15}N -detected TROSY experiment¹¹ and increases the longitudinal relaxation within the system by only exciting a subset of spins (pulse scheme Fig 1). Therefore, all pulses on the ^1H channel were replaced by band-selective pulses. The bandwidth of the proton pulses was chosen to cover only the imino-chemical shift range between 15 ppm and 9 ppm (~ 5000 Hz) where no other protons of the RNA resonate. Further, it ensures that the water resonance is unperturbed and aligns along the z-axis at all times during the experiment providing a reservoir of fast exchanging protons in magnetic equilibrium⁴³. It is necessary to achieve pure in-phase excitation with a single pulse to avoid significant phase corrections in the indirect ^1H -dimension. Therefore, EBurp2⁴⁴ shapes were used as selective 90° pulses. Further, due to the short inter-scan delay (0.2 s), the field strength of the carbon decoupling during acquisition was reduced by 50% compared to the standard TROSY experiment (from 3.6 kHz to 1.8 kHz). The use of shaped 180° -pulses for the ^{15}N -channel is non-essential as there is no sensitivity increase detected. Pulses on ^{15}N were

either applied as hard 180° -pulses or as band-selective Reburp2 shapes covering a bandwidth of ~ 3600 Hz (44 ppm).

Comparison of the ^{15}N -detected HSQC³⁷, TROSY¹¹, and BEST-TROSY experiment reveals the presence of all expected imino resonances in all three experiments (Fig 2 B-D). The HSQC spectra additionally show all expected cytidine amino-resonances (Suppl. Fig 1). Only the guanosine and adenosine amino-resonances that are also difficult to observe in ^1H -detected experiments could not be observed in the ^{15}N -detected HSQC spectra.

The imino-nitrogens exhibit the narrowest line widths in the HSQC experiment. Those nuclei involved in stable Watson-Crick base pairs have a mean ^{15}N -LW(HSQC) = 4.9 ± 0.6 Hz in this experiment, whereas for the two TROSY experiments the measured width is larger (^{15}N -LW(TROSY) = 6.1 ± 0.8 Hz and ^{15}N -LW(BEST-TROSY) = 6.4 ± 0.7 Hz). More strikingly, the difference is even larger for the N1-nitrogen of residue G9. Here, the ^{15}N -LW(HSQC) is 4.9 Hz, whereas in both TROSY experiments larger line widths (^{15}N -LW(TROSY) = 12.5 Hz and ^{15}N -LW(BEST-TROSY) = 11.5 Hz) are measured.

Furthermore, the imino signal of G9 also exhibits the highest relative intensity in the ^{15}N -detected HSQC experiment compared to the other experiments, as shown in the 1D rows of Fig 2 A-D. Both, the high relative intensity and the narrow line width are most probably mainly due to reduced susceptibility to base catalyzed solvent exchange during the acquisition time, where for the HSQC-experiment a pure inphase ^{15}N coherence evolves. From this observation for residue G9 we conclude a principally higher tolerance to solvent exchange of the ^{15}N -detected HSQC experiment.

Nevertheless, within the different ^{15}N -detected experiments, the relative S/N ratio per unit time increases three-fold from the HSQC to the BEST-TROSY experiment ($S/N^{15\text{N-HSQC}} = 1$; $S/N^{15\text{N-TROSY}} = 1.4$; $S/N^{15\text{N-BEST-TROSY}} = 2.9$; Fig 2 A-D). Further, the overlay of 1D rows for the ^{15}N -detected TROSY and BEST-TROSY experiments (Suppl. Fig 1) shows a comparable S/N ratio for the two spectra even though twice as many scans (112 instead of 64) were acquired for the TROSY experiment.

Having established the BEST-TROSY as the most sensitive ^{15}N -detected H-N correlation experiment for RNA molecules, we compare this experiment to its ^1H -detected counterpart.

Optimal acquisition times for the ^1H -detected BEST-TROSY experiment were derived similarly to the ^{15}N -detected experiments from the determined T_2 times and are 0.3 s ($3 \cdot T_2$) in the direct ^1H - and ~ 0.4 s ($1.26 \cdot T_2$) in the indirect ^{15}N -dimension. To achieve the same resolution for the nitrogen resonances, both, the ^1H - and the ^{15}N -detected experiment were recorded with $aq_{t1}(^{15}\text{N}) = aq_{t2}(^{15}\text{N}) = 0.3$ s ($1 \cdot T_2$). As described above, the acquisition time in the indirect ^1H -dimension of the ^{15}N -detected experiment is reduced to $1.26 \cdot T_2 = 0.126$ s; this serves the purpose of this study, as we focus on evaluating resolution effects along ^{15}N -dimensions.

Table 1 Acquisition parameters for ^1H - and ^{15}N -detected BEST-TROSY experiments for the 14 nt RNA.

Parameter	^1H -detected experiment	^{15}N -detected experiment	comment
aq _{t1}	0.3 s	0.126 s	$1 \cdot T_2$ and $1.26 \cdot T_2$
aq _{t2}	0.3 s	0.3 s	$3 \cdot T_2$
sw _{F1}	1946 Hz	3441 Hz	
td _{F1}	1168	867	
ns	2	32	
experimental time	0.5 h	5 h	
S/N	70 / 30	20 / 10	mean / G9

To deconvolute peaks for the extraction of line width parameters we aim at S/N ratios ≥ 10 in both experiments. This is reached with 2 and 32 transients per FID for the ^1H - and ^{15}N -detected BEST-TROSY experiment, respectively. These settings of acquisition parameters, as summarized in Table 1, result in experimental times of ~ 0.5 h and ~ 5 h for the ^1H - and ^{15}N -detected experiments, respectively. This clearly identifies the ^1H -detected BEST-TROSY experiment as the more sensitive H-N correlation experiment. The resolution in both experiments is equally high in the ^{15}N -dimension and yields at our given sw(^{15}N) of 35 ppm a resolution of 1.7 Hz, allowing to resolve small homo-nuclear couplings present in RNA's nucleobases (Fig 2 A-C).

Application of the ^{15}N -detected BEST-TROSY experiment to increasingly large RNAs

As the promise of ^{15}N -detection lies in narrow line width resulting from the slower decay of the ^{15}N -signals, we analyzed ^1H - and ^{15}N -detected BEST-TROSY spectra for a total of five different RNA molecules between 14 nt and 329 nt (Figs 2-4), corresponding to molecular weights from 5 kDa to 100 kDa.

Predicted rotational correlation times for RNAs with known three dimensional structures (using HYDRONMR⁴⁵) range from 3 ns for small hairpins up to 60 ns for the 108 nt T-shaped IRES element⁴⁶. Based on these parameters of molecular tumbling, the calculated ^1H -R₂ relaxation rates are by a factor of 2 larger than the corresponding ^{15}N -R₂ rates for RNAs containing only 40 nt (Fig 5 A). The experimental line widths confirm the theoretical predictions (Fig 5 A) that the signals stay sharper for the ^{15}N - than for the ^1H -dimension with increasing molecular weight. While the average ^1H -line widths increases 4-fold from 14 nt to 329 nt the average ^{15}N -line widths only increases by a factor of two (Fig 5 B). Further, a differential line width effect for the two Watson-Crick base pairs could be detected. For every RNA investigated here, signals for AU base pairs are sharper than signals for GC base pairs with respect to both ^1H - and ^{15}N -line width (Fig 5 C and D). The simulation of transverse relaxation rates shows that with increasing rotational correlation time, relaxation becomes more prominent for GC than for AU base pairs in both the $^1\text{H}^{\text{N}}$ - and the $^{15}\text{N}^{\text{H}}$ -TROSY components (Fig 5 A). This arises on the one hand from differences in chemical shift anisotropies (CSA) of imino ^{15}N and ^1H for GC and AU base pairs, respectively. Here, for example, the absolute value for the $^{15}\text{N}^{\text{H}}$ -CSA of a GC base pair is $\sim 10\%$ higher than the corresponding CSA for AU base pairs (Suppl. Table 1) leading to increased

$^{15}\text{N}^{\text{H}}$ transverse relaxation rates for GC base pairs^{47,48}. On the other hand, different $^1\text{H}^{\text{N}}\text{-}^1\text{H}$ distances for GC and AU base pairs result in different dipole-dipole relaxation and concomitantly higher $^1\text{H}^{\text{N}}$ transverse relaxation rates for GC base pairs.

The analysis reveals for every RNA smaller than 100 kDa that the ^{15}N -line widths are lower than 13 Hz. This in conjunction with the high spectral resolution in the ^{15}N -dimension leads to resolution of a pseudo-doublet structure of the imino-nitrogen resonances with the ^{15}N -detected BEST-TROSY experiment (see Fig 2 B and C). This splitting can also be resolved for a signal in the ^1H -detected BEST-TROSY experiment while recording the experiment with the same acquisition time in the indirect dimension by executing an unusual high number of points (see Fig 2 A, Table 1). In Watson-Crick type base pairs, uridines and guanosines exhibit a hydrogen-bond scalar coupling $^2\text{h}J_{\text{N}1\text{N}3}/^2\text{h}J_{\text{N}3\text{N}1}$ of $\sim 6\text{-}7$ Hz,⁴⁹ which is larger than the intranucleobase $^2J_{\text{N}3\text{N}1}/^2J_{\text{N}1\text{N}2}$ scalar coupling of 2.2 Hz⁵⁰. These interactions – that are indirectly detectable in HNN-COSY experiments⁴⁹ – result in a pseudo-doublet coupling pattern. For the 14 nt hairpin RNA, this coupling is detectable for the resonances of all nucleobases involved in stable Watson-Crick base pairs (U11, G2, G10 and G12) for the ^{15}N -detected BEST-TROSY experiment and for U11 in the ^1H -detected BEST-TROSY experiment using the same theoretical resolution in the respective ^{15}N -dimension.

The same type of cross hydrogen bond scalar coupling can also be directly detected in the spectra of the 127 nt riboswitch RNA (Fig 3). The close-up of the spectra shows an intermolecular $^2\text{h}J_{\text{NN}}$ coupling on the signal of residue U51, which is the coupling between this residue and the ^{13}C - ^{15}N -labeled ligand adenine (structural features of the ligand binding site are given in Fig 3 C). This splitting is not observed if the H-bond acceptor is either not ^{15}N isotope labelled (as for all other residues in the 127 nt riboswitch) or if the hydrogen bond acceptor is an oxygen atom (as it is the case for residue G9 in the 14 nt hairpin RNA). In contrast to the inter-nucleotide coupling, a splitting due to the intra-nucleotide $^2J_{\text{NN}}$ coupling is not resolved. Even for the smallest RNA the line width in the ^{15}N -dimension (AU base pair: 5.3 Hz; GC base pair: 6.8 Hz, as measured in ^{15}N BEST-TROSY) exceeds the intra-base scalar coupling, rendering a direct resolution of this coupling impossible.

Variations in line width

We also observe a significant variation of signal line widths for each investigated RNA. This effect is more prominent for ^1H - than for ^{15}N -line widths. For example, for the three stably structured RNAs, the 14 nt hairpin RNA, the 74 nt Spinach RNA and the 127 nt adenine-sensing riboswitch (holo-conformation), the ^1H -line widths exhibit a range of 3.5 Hz, 17.2 Hz and 19.3 Hz, whereas for ^{15}N the range is only 1.54 Hz, 5.4 Hz and 6.9 Hz. Variations for the ^1H line widths are mostly due to solvent exchange. Already for the 14 nt hairpin RNA the variation in the ^1H exchange rate, as measured by ^1H -detected inversion recovery experiments⁵¹, exceeds 2 Hz for Watson-Crick base pairs. Exchange rates range between ~ 1 s⁻¹ and 3.5 s⁻¹ (2.3 s⁻¹ \pm 0.7 s⁻¹ (U11), 2.1 s⁻¹ \pm 0.7 s⁻¹ (G2), 0.9 s⁻¹ \pm 0.6 s⁻¹ (G12) and 3.4 s⁻¹ \pm 0.8 s⁻¹ (G10)). Thus, the exchange of the imino hydrogen atoms with water contributes up to 25% of the line width of the imino hydrogen atoms in Watson-Crick base pairs. Similarly, the origin of the sharp lines of the G-quadruplex signals in the ^1H -dimension of the 74 nt spinach RNA originate from a particularly small exchange rate. These imino protons

can still be detected hours after a transfer of the RNA into D₂O⁵². The solvent exchange contribution is also responsible for the broader ¹H-line width of the UU wobble base pair in comparison to the GC base pair (Fig 5 C, Fig 4 J and K) within the 329 nt CUG repeat RNA. Generally in Watson-Crick helices, GC base pairs are more stable and the exchange rate of the respective imino proton is lower than the one in UU wobble base pairs⁵³.

Notably, all measured ¹⁵N-line widths are increased in comparison to simulated values (Fig 5 A and B). The ¹⁵N experimental line width can be affected by solvent exchange as it is derived from the shape of a TROSY signal that arises from an antiphase operator carrying proton polarization²³. Further, in addition to the already discussed homo-nuclear ²J_{NN} couplings unresolved scalar couplings to remote protons, e.g. ³J_{H5N3} in uridines and ³J_{H21N1} in guanines can increase the line width⁵⁰. And finally, conformational averaging on an intermediate exchange time-scale can also lead to a broadening of the ¹⁵N-line widths. For Watson-Crick base pairs, the chemical shift range of imino-nitrogens spans 5.4 ppm and 4.4 ppm for guanine and uridine, respectively. When considering all base pairs containing the keto-tautomeric form, the span is increased to 8 ppm and 10 ppm, respectively (see Suppl. Fig 2 C). In turn, this means that conformational exchanges with rates up to 0.8 kHz, could lead to broadening of the affected resonances at the given field (80 MHz for ¹⁵N). Such processes are indeed reported for several biological active RNA molecules, where exchange rates between different conformational states from 100 Hz up to ~9 kHz are observed and where the population of the second states can reach up to ~10%⁵⁴. Dependent on the rate of the underlying exchange processes and the difference of resonance frequencies the particular sites can be in the fast-to-intermediate or intermediate-to-slow regime, which would be distinguishable by a differential field dependency of the line width.

Effect of magnetic field strength

Not only the exchange contributions exhibit a dependence on the applied magnetic field but also the relaxation behavior of TROSY component (Suppl. Fig 5)^{11,55}. Therefore, the H-N correlation experiments were repeated on a 950 MHz (22.3 T) NMR spectrometer equipped with a TXO probe for the 14 nt, 127 nt and 329 nt RNAs, respectively (Fig 6 A, B and D). Parameters including the number of scans per increment were not changed in comparison to the spectra recorded on the 800 MHz spectrometer (18.8 T), while the number of points were adapted from 1702 (sweep width 2841 Hz) to 2020 (sweep width 3370 Hz) according to the higher field. According to predictions, only minor improvements in ¹⁵N-resolution (~10%) are to be expected for RNAs of a rotational correlation time of 60 ns by measuring at the higher magnetic field (Suppl. Fig 5). Those changes are below the maximal resolution of 1.7 Hz achieved in the experiment. Even for the large RNAs in our study (127 nt and 329 nt RNAs), no resolution improvement could be detected in comparison to spectra recorded at 800 MHz (Fig 6 C). The S/N-ratio, however, is increased by a factor of ~1.5 due to better ¹⁵N-sensitivity. This increase in sensitivity results from the higher magnetic field strength as predicted^{11,55} in combination with utilizing a ¹⁵N-optimized TXO probe, which increases sensitivity by an additional 30% in comparison to a ¹³C-optimized probe.

It is thus necessary to go to even larger rotational correlation times or magnetic field strength to be able to detect resolution improvement as the ¹⁵N^H optimum for RNA is at 29.5 T (GC) and 32.8 T (AU). The magnetic

field strength optimum for the imino proton of RNA depends strongly on its chemical shift anisotropy for which various values are reported in the literature⁴⁸. Using the calculated values from Czernek *et al*⁶⁶ the respective minima of the ¹⁵N-line width would be 17.7 T (AU) and 19.2 T(GC). Field strength optima are not equal for GC and AU base pairs due to differences in the listed parameters (Suppl. Table 1). Further, at closer inspection of the ¹⁵N-line width determined, we actually observe an increase at higher field, indicating that processes that are closer to the intermediate exchange regime at 22.3 T exist in all RNAs examined (Fig 6 C).

Conclusion

In this work, we applied ^{15}N -detected HSQC and TROSY¹¹ experiments to various RNA molecules. An improved pulse sequence (^{15}N -detected BEST-TROSY) is implemented that saves a factor of 2 in measurement time with respect to the previously published scheme. In comparison to the ^1H -detected BEST-TROSY experiment the three ^{15}N -detected H-N correlation experiments exhibit a lower S/N-ratio for a 14 nt RNA while resolution in the direct and indirect ^{15}N -dimensions is similarly high when using identical acquisition parameters.

Further, BEST-TROSY experiments were conducted on a set of RNA molecules where the line width behavior was investigated in dependence of molecular size, base pair type as well as chemical and conformational exchange. Here, ^{15}N -line widths stay sharper with increasing chain length than the lines in the ^1H -dimension. This result is interesting since signal overlap for large molecules is one of the main problems in biomolecular NMR spectroscopy and techniques able to characterize RNAs of higher molecular weight are needed. Based on the observable trend of line widths, conducting ^{15}N -detected experiments could be a start towards that goal since the dimension with the intrinsically high resolution and therefore the one where more data points need to be recorded is the direct dimension, which comes for free in terms of measurement time. This high ^{15}N -resolution shows for both, the ^1H - and the ^{15}N -detected BEST-TROSY experiments, in the ability to extract $^{2h}J_{\text{NN}}$ couplings, since the corresponding signals of Watson-Crick type base pairs and ligand binding sites exhibit a pseudo doublet. Watson-Crick and wobble base pairs thus can be reliably distinguished, not only based on chemical shift differences, but also by evaluating whether the respective signal exhibits a pseudo doublet due to hydrogen bond-mediated $^{2h}J_{\text{NN}}$ scalar coupling.

With this work, we also verified experimentally the different relaxation behavior of the imino signals corresponding to AU and GC Watson-Crick base pairs. GC base pairs give rise to broader resonances due to their higher transverse relaxation rates originating from the different ^{15}N chemical shift anisotropies. Further, the ^{15}N -line width measurements at different field strength hint at exchange processes in RNAs that obscure the relaxation interference benefits at ultra-highfield spectrometers.

Unfortunately, the ^{15}N -detected BEST-TROSY experiment does not show additional signals and is less sensitive compared to the ^1H -detected experiment for all RNAs investigated in this study. So for RNA investigations, the advantage of ^{15}N -detection over ^1H -detection as it was found for protein NMR¹² was not replicated under the experimental conditions applied here. Yet, a higher tolerance to imino proton exchange is observed for the ^{15}N -detected HSQC experiment, but at the cost of lowest sensitivity.

In cases where correlations between the imino nitrogen and its attached proton are concealed by exchange e.g. in flexible regions of RNA, ^{13}C -detected CN-correlated experiments are the method of choice. The viability of such an approach, including characterization of partial hydrogen bonding, was previously shown for RNAs, dissolved both in D_2O or in H_2O .¹⁶ Therefore, the ^{13}C -detected NC correlation and the ^{15}N -detected H-N correlation experiments represent complementary approaches to extend the limits of NMR spectroscopy of RNA.

Acknowledgements

Matthias Görlach from the Core Facilities and Services (CS Protein Production) of the Fritz Lipmann Institute, Jena, is gratefully acknowledged for providing the 329 nt RNA.

This work was funded by the German funding agency (DFG) in Collaborative Research Center 902: Molecular principles of RNA-based regulation and in Graduate College: CLIC (GRK1982). Financial support by European access program (iNEXT) is gratefully acknowledged. Harald Schwalbe is member of the DFG-funded Cluster of Excellence: macromolecular complexes (EXC115). Robbin Schnieders is supported by the Fonds of the Chemical Industry. Work at BMRZ is supported by the state of Hesse. We acknowledge access to the 950 MHz spectrometer of the Astbury BioStructure Laboratory BioNMR Facility (University of Leeds) which was funded by the University of Leeds.

Fig 1: Pulse sequence of the ^{15}N -detected BEST-TROSY experiment^{11,23}. 90° pulses are shown as narrow filled bars, while rectangular 180° pulses are represented as wide unfilled bars. Semi-elliptic shapes correspond to gradient and selective pulses (90° ; ^1H : EBurp2.tr, EBurp2 and EBurp2.tr⁴⁴, 180° ; ^1H : Reburp2⁴⁴, 180° ; ^{15}N : Reburp2⁴⁴). ^{13}C nuclei during acquisition were decoupled using asynchronous GARP4 decoupling sequences⁵⁷. Unless noted otherwise, the pulse phase is x . Phases are: $\varphi_1 = y, -y, -x, x/-y, y, x, -x$ and $\varphi_{\text{rec}} = x, -x, -y, y$. The delay Δ is set to $(2 \cdot J(\text{NH}))^{-1} = 5.6$ ms. Gradient pulses are applied with a smoothed square amplitude (SMSQ10.100) for 1 ms and with strengths of 31% (g_1) and 19% (g_2) (100% corresponds to 53 G/cm). Selective pulses were applied with the following length at 800 MHz: 1275 μs (EBurp2), 1050 μs (Reburp2, ^1H) and 1500 μs (Reburp2, ^{15}N).

Fig 2: Comparison of a ^1H -detected BEST-TROSY spectrum (**A**) with **B** a ^{15}N -detected TROSY as well as **C** a ^{15}N -detected BEST-TROSY and **D** a ^{15}N -detected HSQC spectrum of a 14 nt RNA hairpin at 298 K. All spectra were recorded at 800 MHz (18.8 T). For better comparison, the ^1H -detected experiment was conducted on a spectrometer equipped with a TCI probe and all three of the ^{15}N direct-detected experiments were recorded on a spectrometer equipped with a TXO probe. All spectra include close-ups of the signals for U11, G2 and G9 to show whether the $^2\text{h}J_{\text{NN}}$ coupling can be resolved. Spectrum **A** has been recorded with a spectral width of 24 ppm respectively in both dimensions. Carrier frequencies for ^1H , ^{13}C and ^{15}N were set to 4.7 ppm, 150 ppm and 153 ppm respectively. Hard pulses were applied with field strength of 22.9 kHz (^1H), 22.3 kHz (^{13}C) and 7.6 kHz (^{15}N). Acquisition times were 0.3 s (^1H) and 0.3 s (^{15}N). With 32 scans per increment and a relaxation delay of 0.3 s, the final measurement time was 8 h. Both spectra **B** and **C** were recorded with a spectral width of 35 ppm (^{15}N) and 4.3 ppm (^1H) and with carrier frequencies of 155 ppm for nitrogen, 160 ppm for carbon and 11.675 ppm for ^1H channels respectively. Hard pulses were applied with field strength of 6.4 kHz (^{15}N) and 17.5 kHz (^1H). GARP4 decoupling sequences on carbon nuclei were conducted with 1.8 kHz. The acquisition times were 0.3 s for nitrogen and 0.126 s for protons. The ^{15}N -detected TROSY experiment (**B**) has been recorded with 112 scans per increment and with a relaxation delay of 1 s the resulting measurement time was 1 d 14 h. For the ^{15}N -detected BEST-TROSY experiment **C** 64 scans per increment were recorded and with a relaxation delay of 0.3 s followed a total measurement time of 11 h. **D** The 2D HSQC spectrum of the imino region was recorded with spectral widths of 35 ppm and 4.4 ppm in the direct ^{15}N - and indirect ^1H -dimension, respectively. The acquisition times were 0.3 s and 0.04 s, respectively. The acquisition time in the indirect dimension was reduced to save measurement time, which only enables resolution comparison in the direct ^{15}N -dimension. Carrier frequencies for ^{15}N , ^1H and ^{13}C were set to 155 ppm, 11.8 ppm and 150 ppm. Hard pulses were applied with field strength of 6.4 kHz (^{15}N), 17.5 kHz (^1H) and 21.9 kHz (^{13}C). Conducting 128 scans per increment with an inter-scan delay of 1 s resulted in an overall experimental time of 15 h.

Fig 3: A) Secondary structure of the 127 nt RNA in the ligand-bound holo conformation³². **B)** Close-ups of the ¹H-detected (top) and ¹⁵N-detected (bottom) BEST-TROSY spectra of the 127 nt adenine-sensing riboswitch in the presence of 5 mM Mg²⁺ and 2 equivalents of adenine at 298 K (for full spectrum see Suppl. Fig 2). The spectra were both recorded at 800 MHz (18.8 T) NMR spectrometers, one equipped with a TCI probe for the ¹H-detected experiment and the other one equipped with a TXO probe for the nitrogen-detected TROSY experiment. Carrier frequencies for the ¹H-detected BEST-TROSY experiment were 4.7 ppm (¹H), 101 ppm (¹³C) and 153 ppm (¹⁵N) respectively. The spectral widths were chosen to be 25 ppm (¹H) and 28 ppm (¹⁵N) respectively. Hard pulses on ¹H, ¹³C and ¹⁵N were applied with field strengths of 21.7 kHz, 22.3 kHz and 7.6 kHz respectively. The experiment was conducted with 64 number of scans and acquisition times of 0.3 s in the direct and 0.3 s in the indirect dimension. With a relaxation delay of 0.5 s resulted a total time for the experiment of 20 h 30 min. The ¹⁵N detected BEST-TROSY experiment was recorded with carrier frequencies for ¹⁵N, ¹³C and ¹H of 155 ppm, 120 ppm and 12.175 ppm respectively. Spectral widths of 35 ppm in the direct and 5.2 ppm in the indirect dimension were covered. Hard pulses were carried out using field strength of 7.3 kHz (¹⁵N), 21.9 kHz (¹³C) and 21.3 kHz (¹H). The number of scans per increment was set to 576 and the relaxation delay to 0.2 s. The experiment was recorded for 20 h with acquisition times of 0.3 s in the ¹⁵N and 0.03 s in the ¹H-dimension. **C)** Schematic representation of adenine-binding to residues U51 and U74⁵⁸. The ²hJ_{NN}-couplings are marked.

Fig 4: ¹H- and ¹⁵N-detected BEST-TROSY spectra of the 40 nt¹⁶, 47 nt²⁷, 74 nt³⁰ and 329 nt⁸⁵ RNAs with their respective secondary structure and labelling pattern. All spectra were recorded at 800 MHz (18.8 T) at 298 K. For better comparison, the ¹H-detected experiments were conducted on a spectrometer equipped with a TCI-probe and all of the ¹⁵N direct-detected experiments were recorded on a spectrometer equipped with a TXO probe. The following parameters stay the same for all RNAs within the ¹H-detected experiments: The spectral width in the ¹H-dimension was set to 24 ppm and carrier frequencies for ¹H and ¹³C were 4.7 ppm and 101 ppm, respectively. Hard pulses were applied with field strength of 22.3 kHz (¹³C) and 7.6 kHz (¹⁵N) and the acquisition time in the direct ¹H-dimension was 0.3 s. For the ¹⁵N-detected BEST-TROSY experiments the following parameters were identical for all constructs: The spectral width in the ¹⁵N-dimension was set to 35 ppm, while the carrier frequencies were 155 ppm (¹⁵N) and 150 ppm (¹³C). During the acquisition (0.3 s) carbon decoupling was performed using GARP4 sequences with a field strength of 1.8 kHz. For detailed parameters of the experiments see Supporting Information. **A)** ¹H-detected and **B)** ¹⁵N-detected BEST-TROSY spectra of the 40 nt RNA. **C)** Secondary structure of the 40 nt long RNA with ¹³C-¹⁵N-labeled uridines. **D)** ¹H-detected and **E)** ¹⁵N-detected BEST-TROSY spectra of the 47 nt RNA. **F)** Secondary structure of the 47 nt long RNA with ¹³C-¹⁵N labeled uridines. **G)** ¹H-detected and **H)** ¹⁵N-detected BEST-TROSY spectra of the 74 nt RNA. **I)** Secondary structure of the 74 nt long spinach RNA with ¹⁵N labeled guanosines and uridines. **J)** ¹H-detected and **K)** ¹⁵N-detected BEST-TROSY spectra of the 329 nt RNA. **L)** Secondary structure of the 329 nt CUG repeat RNA where all nucleotides are ¹³C-¹⁵N labeled.

Fig 5: A) Transverse relaxation rates in dependence of the rotational correlation time for the ¹⁵N^H and the ¹H^N TROSY components. Here, AU and GC Watson-Crick base pairs were calculated separately with corresponding parameters (Suppl. Table 1) and equations 1-12 (Suppl. Material). For four RNAs with 14, 37, 67 and 108 nucleotides (pdb 2KOC⁴⁰, 2LHP⁵⁹, 2NC1⁴⁶ and 2NBX⁴⁶) rotational correlation times were calculated from their pdb structure using HYDRONMR⁴⁵.

B) Trend for the ^1H - and ^{15}N -line width at half height for the following RNA constructs: 14 nt, 40 nt, 47 nt, 74 nt, 127 nt (for apo- and holo-states) and 329 nt. The light colored points represent all the single line widths measured for the constructs in the respective dimension and the bright colored points are the mean values of the line width. The error represents the maximal theoretical resolution of the spectra in the respective direct dimension (1.7 Hz for both, $^1\text{H}^{\text{det}}$ and ^{15}N -detected experiments). **C)** ^1H -Line widths at half height for different base pair groups plotted against the number of nucleotides for the constructs; AU Watson-Crick base pairs (filled bars), GC Watson-Crick base pairs (open bars), G-quadruplex (up-hashed), tertiary interactions (down-hashed) and UU base pair (dashed). **D)** ^{15}N -Line widths at half height for different base pair groups (marked as in C).

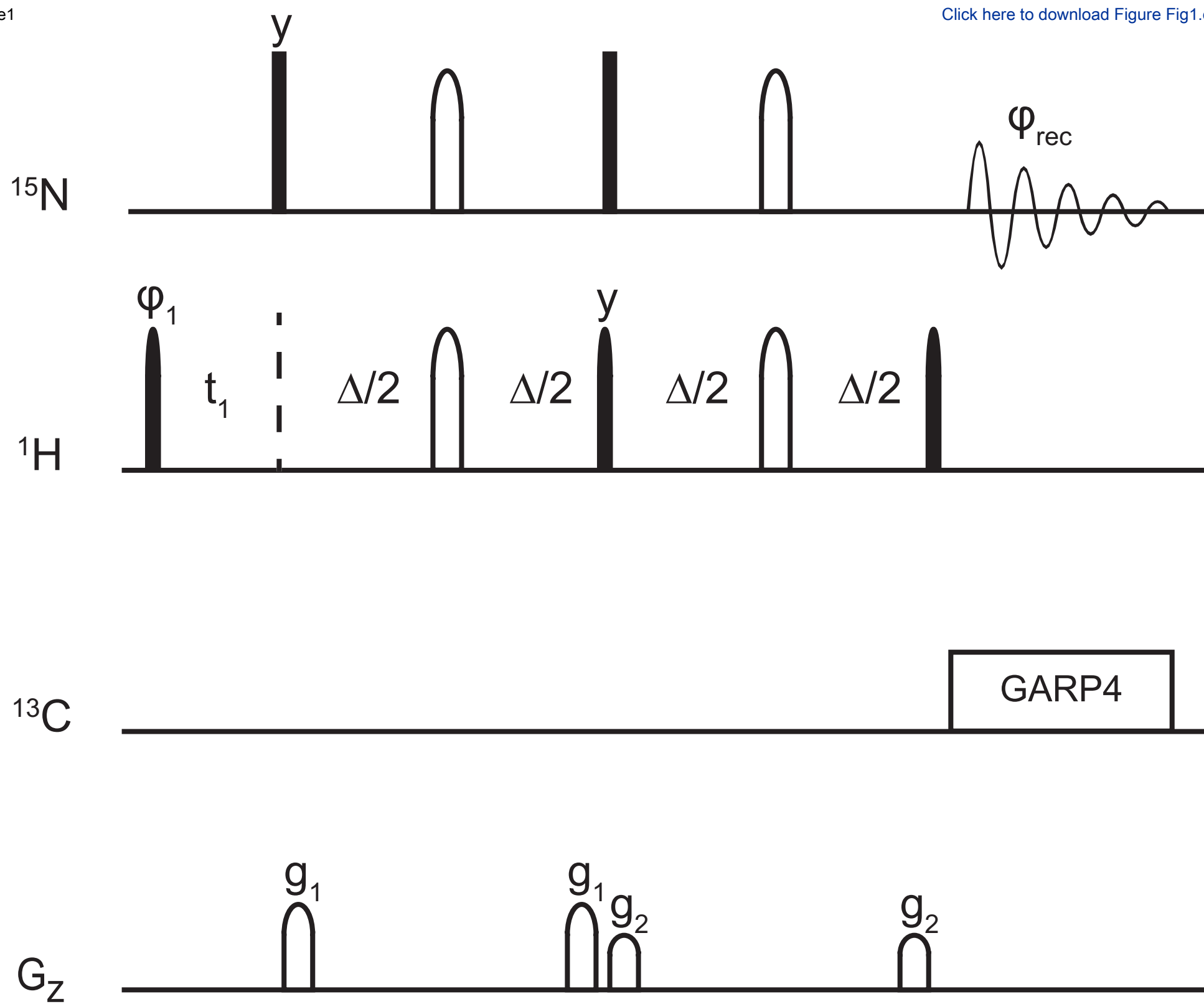
Fig 6: All spectra were recorded on a 950 MHz spectrometer featuring a TXO probe at 298 K. **A)** ^{15}N -detected BEST-TROSY spectrum of the 14 nt hairpin RNA with UUCG tetraloop⁴⁰. It was recorded with spectral widths of 35 ppm in the direct ^{15}N - and 4.3 ppm in the indirect ^1H -dimension. Carrier frequencies for ^{15}N , ^{13}C and ^1H were set to 155 ppm, 150 ppm and 4.7 ppm, respectively. Hard pulses were applied with field strength of 7.1 kHz (^{15}N), and 21.1 kHz (^1H). Acquisition times were set to 0.3 s in the direct ^{15}N -dimension and 0.06 s in the indirect ^1H -dimension, respectively. GARP4 decoupling sequences on carbon nuclei were conducted with 3.1 kHz. With 64 scans per increment and a relaxation delay of 0.3 s the final measurement time was 6 h. **B)** ^{15}N -detected BEST-TROSY spectrum of the 329 nt CUG repeat⁸⁵. It was recorded with spectral widths of 35 ppm in the direct ^{15}N - and 3.5 ppm in the indirect ^1H -dimension. Carrier frequencies for ^{15}N , ^{13}C and ^1H were set to 155 ppm, 150 ppm and 4.7 ppm, respectively. Hard pulses were applied with field strength of 7.1 kHz (^{15}N), and 19.8 kHz (^1H). Acquisition times were set to 0.3 s in the direct ^{15}N -dimension and 0.03 s in the indirect ^1H -dimension, respectively. GARP4 decoupling sequences on carbon nuclei were conducted with 3.1 kHz. With 640 scans per increment and a relaxation delay of 0.3 s the final measurement time was 22 h. **C)** Plot of line widths extracted from spectra measured at 950 MHz against line width extracted from 800 MHz spectra from the 14 nt (red), 127 nt (green) and 329 nt (blue) RNAs. Major dots represent the mean values and are shown with error bars (resolution limit), minor dots represent the individual values for each measured resonance. Theoretical predictions for linewidths of GC base pairs (dashed line) and AU base pairs (solid line) are included. **D)** ^{15}N -detected BEST-TROSY spectrum of the 127 nt adenine sensing riboswitch³² in the holo-state. It has been recorded with spectral widths of 35 ppm in the direct ^{15}N - and 5.0 ppm in the indirect ^1H -dimension. Carrier frequencies for ^{15}N , ^{13}C and ^1H were set to 155 ppm, 150 ppm and 4.7 ppm, respectively. Hard pulses were applied with field strength of 7.1 kHz (^{15}N), and 19.8 kHz (^1H). Acquisition times were set to 0.3 s in the direct ^{15}N -dimension and 0.02 s in the indirect ^1H -dimension, respectively. GARP4 decoupling sequences on carbon nuclei were conducted with 3.1 kHz. With 576 scans per increment and a relaxation delay of 0.3 s the final measurement time was 21 h.

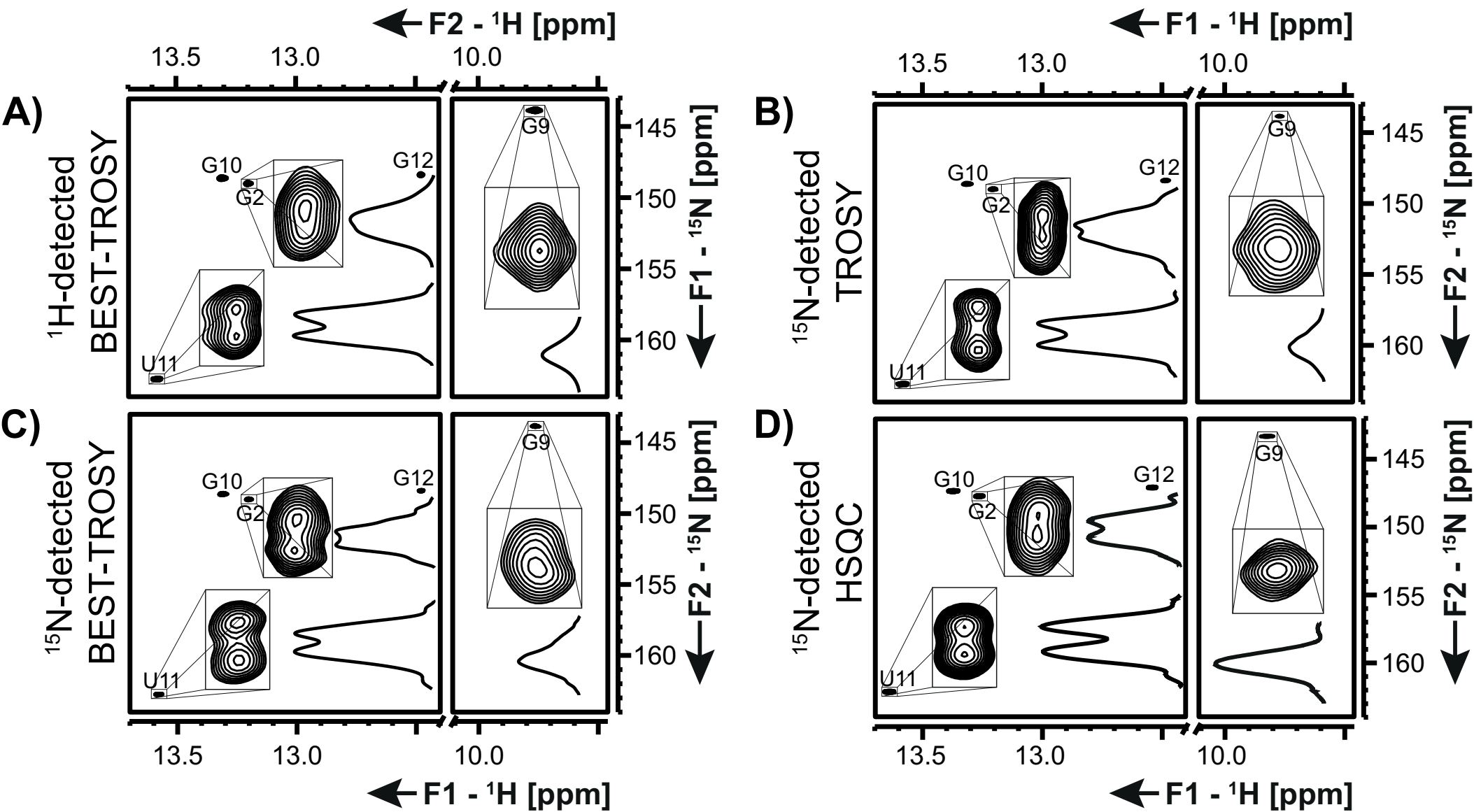
References

1. Alexandrescu, A. T., Loh, S. N. & Markley, J. L. Chemical Exchange Spectroscopy Based on Carbon-13 NMR . Applications to Enzymology and Protein Folding. *J. Magn. Reson.* **87**, 523–535 (1990).
2. Bermel, W., Bertini, I., Felli, I. C., Piccioli, M. & Pierattelli, R. ¹³C-detected protonless NMR spectroscopy of proteins in solution. *Prog. Nucl. Magn. Reson. Spectrosc.* **48**, 25–45 (2006).
3. Serber, Z., Richter, C., Moskau, D., Bo, J., Gerfin, T., Marek, D., Baselgia, L., Laukien, F., Stern, A. S., Hoch, J. C. & Dötsch, V. New Carbon-Detected Protein NMR Experiments Using CryoProbes. *J. Am. Chem. Soc.* **122**, 3554–3555 (2000).
4. Kovacs, H., Moskau, D. & Spraul, M. Cryogenically Cooled Probes — A Leap in NMR Technology. *Prog. Nucl. Magn. Reson. Spectrosc.* **46**, 131–155 (2005).
5. Felli, I. C. & Pierattelli, R. Novel methods based on proteins ¹³C detection to study intrinsically disordered proteins. *J. Magn. Reson.* **241**, 115–125 (2014).
6. Pervushin, K. & Eletsky, A. A new strategy for backbone resonance assignment in large proteins using a MQ-HACACO experiment. *J. Biomol. NMR* **25**, 147–152 (2003).
7. Bermel, W., Bertini, I., Felli, I., Piccioli, M. & Pierattelli, R. ¹³C-detected protonless NMR spectroscopy of proteins in solution. *Prog. Nucl. Magn. Reson. Spectrosc.* **48**, 25–45 (2006).
8. Sadek, M. & Brownlee, R. T. C. Study of ¹⁵N-Labeled Paramagnetic Compounds by ¹⁵N-Detected NMR Experiments. *J. Magn. Reson.* **109**, 70–75 (1995).
9. Takeuchi, K., Heffron, G., Frueh, D. P. & Wagner, G. Nitrogen-detected CAN and CON experiments as alternative experiments for main chain NMR resonance assignments. *J. Biomol. NMR* **47**, 271–282 (2010).
10. Gal, M., Edmonds, K. A., Milbradt, A. G., Takeuchi, K. & Wagner, G. Speeding up direct ¹⁵N detection : hCaN 2D NMR experiment. *J. Biomol. NMR* **51**, 497–504 (2011).
11. Takeuchi, K., Arthanari, H., Shimada, I. & Wagner, G. Nitrogen detected TROSY at high field yields high resolution and sensitivity for protein NMR. *J. Biomol. NMR* **63**, 1–9 (2015).
12. Takeuchi, K., Arthanari, H., Imai, M. & Wagner, G. Nitrogen-detected TROSY yields comparable sensitivity to proton-detected TROSY for non-deuterated , large proteins under physiological salt conditions. *J. Biomol. NMR* **64**, 143–151 (2016).
13. Fares, C., Amata, I. & Carlomagno, T. ¹³C-Detection in RNA Bases : Revealing Structure - Chemical Shift Relationships. *J. Am. Chem. Soc.* **129**, 15814–15823 (2007).
14. Fiala, R. & Sklenár, V. ¹³C-detected NMR experiments for measuring chemical shifts and coupling constants in nucleic acid bases. *J. Biomol. NMR* **39**, 153–163 (2007).
15. Richter, C., Kovacs, H., Buck, J., Wacker, A., Fürtig, B., Bermel, W. & Schwalbe, H. ¹³C-direct detected NMR experiments for the sequential J-based resonance assignment of RNA oligonucleotides. *J. Biomol. NMR* **47**, 259–269 (2010).
16. Fürtig, B., Schnieders, R., Richter, C., Zetzsche, H., Keyhani, S., Helmling, C., Kovacs, H. & Schwalbe, H. Direct ¹³C-detected NMR experiments for mapping and characterization of hydrogen bonds in RNA. *J. Biomol. NMR* **64**, 207–221 (2016).
17. Lu, K., Heng, X., Garyu, L., Monti, S., Garcia, E. L., Kharytonchyk, S., Dorjsuren, B., Kulandaivel, G., Jones, S., Hiremath, A., Divakaruni, S. S., Lacotti, C., Barton, S., Tummlillo, D., Husic, A., Edme, K., Albrecht, S., Telesnitsky, A. & Summers, M. F. NMR Detection of Structures in the HIV-1 5'-Leader RNA That Regulate Genome Packaging. *Science* **334**, 242–245 (2011).
18. Alvarado, L. J., Leblanc, R. M., Longhini, A. P., Keane, S. C., Jain, N., Yildiz, Z. F., Tolbert, B. S., Souza, V. M. D., Summers, M. F., Kreutz, C. & Dayie, T. K. Regio-Selective Chemical-Enzymatic Synthesis of Pyrimidine Nucleotides Facilitates RNA Structure and Dynamics Studies. *ChemBiochem* **15**, 1573–1577 (2014).
19. Wilusz, J. E., Sunwoo, H. & Spector, D. L. Long noncoding RNAs : functional surprises from the RNA world. *Genes Dev.* **23**, 1494–1504 (2009).

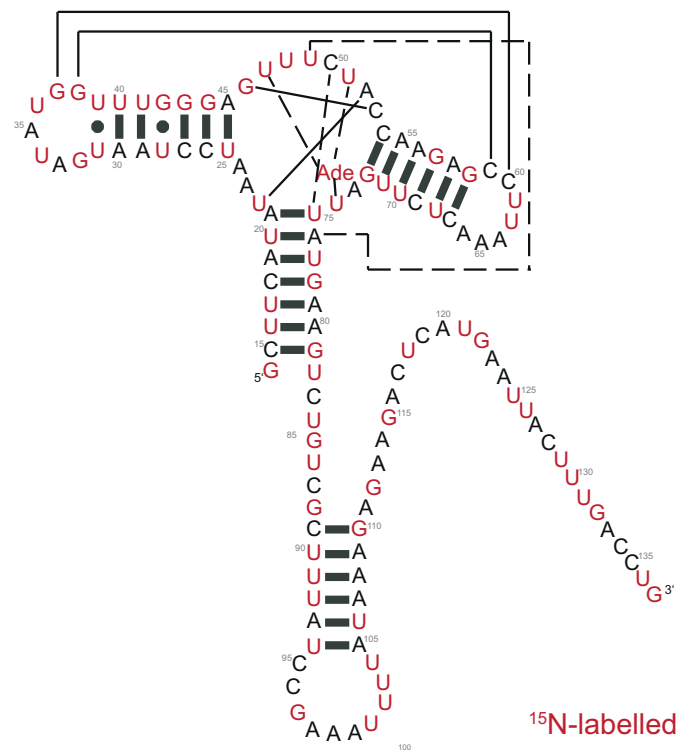
20. Tanaka, Y., Kojima, C., Morita, E. H., Kasai, Y., Yamasaki, K., Ono, A., Kainosho, M. & Taira, K. Identification of the Metal Ion Binding Site on an RNA Motif from Hammerhead Ribozymes Using ^{15}N NMR Spectroscopy. *J. Am. Chem. Soc.* **124**, 4595–4601 (2002).
21. Tanaka, Y. & Ono, A. Nitrogen-15 NMR spectroscopy of N-metallated nucleic acids: insights into NMR parameters and N-metal bonds. *Dalt. Trans.* 4965–4974 (2008). doi:10.1039/b803510p
22. Wang, W., Zhao, J., Han, Q., Wang, G., Yang, G., Anthony, J., Liu, J., Gaffney, B. L. & Jones, R. A. Modulation of RNA Metal Binding Sites by Flanking Bases: ^{15}N NMR Evaluation of GC, Tandem GU, and Tandem GA Sites. *Nucleosides, Nucleotides, and Nucleic Acids* **28**, 424–434 (2009).
23. Pervushin, K., Riek, R., Wider, G. & Wüthrich, K. Attenuated T2 relaxation by mutual cancellation of dipole-dipole coupling and chemical shift anisotropy indicates an avenue to NMR structures of very large biological macromolecules in solution. *Proc. Natl. Acad. Sci.* **94**, 12366–12371 (1997).
24. Fürtig, B., Richter, C., Bermel, W. & Schwalbe, H. New NMR experiments for RNA nucleobase resonance assignment and chemical shift analysis of an RNA UUCG tetraloop. *J. Biomol. NMR* **28**, 69–79 (2004).
25. Guillerez, J., Lopez, P. J., Proux, F., Launay, H. & Dreyfus, M. A mutation in T7 RNA polymerase that facilitates promoter clearance. *Proc. Natl. Acad. Sci. U. S. A.* **102**, 5958–63 (2005).
26. Helmling, C., Keyhani, S., Sochor, F., Fürtig, B., Hengesbach, M. & Schwalbe, H. Rapid NMR screening of RNA secondary structure and binding. 67–76 (2015).
27. Zhao, B., Hansen, A. L. & Zhang, Q. Characterizing Slow Chemical Exchange in Nucleic Acids by Carbon CEST and Low Spin-Lock Field R1 ρ NMR Spectroscopy. *J. Am. Chem. Soc.* **136**, 20–23 (2014).
28. Walker, S. C., Avis, J. M. & Conn, G. L. General plasmids for producing RNA in vitro transcripts with homogeneous ends. *Nucleic Acids Res.* **31**, 1–6 (2003).
29. Silvers, R., Keller, H., Schwalbe, H. & Hengesbach, M. Differential Scanning Fluorimetry for Monitoring RNA Stability. *Chembiochem* **16**, 1109–1114 (2015).
30. Paige, J. S., Wu, K. Y. & Jaffrey, S. R. RNA Mimics of Green Fluorescent Protein. *Science* **333**, 642–646 (2011).
31. Duchardt-Ferner, E., Gottstein-Schmidtke, S. R., Weigand, J. E., Ohlenschläger, O., Wurm, J.-P., Hammann, C., Suess, B. & Wöhnert, J. What a Difference an OH Makes: Conformational Dynamics as the Basis for the Ligand Specificity of the Neomycin-Sensing Riboswitch. *Angew. Chemie - Int. Ed.* **55**, 1527–1530 (2016).
32. Reining, A., Nozinovic, S., Schlepckow, K., Buhr, F., Fürtig, B. & Schwalbe, H. Three-state mechanism couples ligand and temperature sensing in riboswitches. *Nature* **499**, 355–9 (2013).
33. Stoldt, M., Wöhnert, J., Görlach, M. & Brown, L. R. The NMR structure of Escherichia coli ribosomal protein L25 shows homology to general stress proteins and glutamyl-tRNA synthetases. *EMBO J.* **17**, 6377–6384 (1998).
34. Noeske, J., Richter, C., Grundl, M. A., Nasiri, H. R., Schwalbe, H. & Wöhnert, J. An intermolecular base triple as the basis of ligand specificity and affinity in the guanine- and adenine-sensing riboswitch RNAs. *Proc. Natl. Acad. Sci.* **102**, 1372–1377 (2005).
35. Leppert, J., Urbinati, C. R., Häfner, S., Ohlenschläger, O., Swanson, M. S., Görlach, M. & Ramachandran, R. Identification of NH N hydrogen bonds by magic angle spinning solid state NMR in a double-stranded RNA associated with myotonic dystrophy. *Nucleic Acids Res.* **32**, 1177–1183 (2004).
36. Stoldt, M., Wöhnert, J., Görlach, M. & Brown, L. R. The NMR structure of the 5S rRNA E-domain – protein L25 complex shows preformed and induced recognition. *EMBO J.* **18**, 6508–6521 (1999).
37. Bax, A. & Morris, G. A. An Improved Method for Heteronuclear Chemical Shift Correlation by Two-Dimensional NMR. *J. Magn. Reson.* **42**, 501–505 (1981).
38. Favier, A. & Brutscher, B. Recovering lost magnetization: polarization enhancement in biomolecular NMR. *J. Biomol. NMR* **49**, 9–15 (2011).
39. Solyom, Z., Schwarten, M., Geist, L., Konrat, R., Willbold, D. & Brutscher, B. BEST-TROSY experiments for time-efficient sequential resonance assignment of large disordered proteins. *J.*

- Biomol. NMR* **55**, 311–321 (2013).
40. Nozinovic, S., Fürtig, B., Jonker, H. R. A., Richter, C. & Schwalbe, H. High-resolution NMR structure of an RNA model system: the 14-mer cUUCGg tetraloop hairpin RNA. *Nucleic Acids Res.* **38**, 683–94 (2010).
 41. Redfield, A. G. On the Theory of Relaxation Processes. *IBM J. Res. Dev.* **1**, 19–31 (1957).
 42. Rovnyak, D., Hoch, J. C., Stern, A. S. & Wagner, G. Resolution and sensitivity of high field nuclear magnetic resonance. *J. Biomol. NMR* **30**, 1–10 (2004).
 43. Grzesiek, S. & Bax, A. The Importance of Not Saturating H₂O in Protein NMR. Application to Sensitivity Enhancement and NOE Measurements. *J. Am. Chem. Soc.* **115**, 12593–12594 (1993).
 44. Geen, H. & Freeman, R. Band-Selective Radiofrequency Pulses. *J. Magn. Reson.* **93**, 93–141 (1991).
 45. de la Torre, J. G., Huertas, M. L. & Carrasco, B. HYDRONMR: Prediction of NMR Relaxation of Globular Proteins from Atomic-Level Structures and Hydrodynamic Calculations. *J. Magn. Reson.* **147**, 138–146 (2000).
 46. Imai, S., Kumar, P., Hellen, C. U. T., Souza, V. M. D. & Wagner, G. An accurately preorganized IRES RNA structure enables eIF4G capture for initiation of viral translation. *Nat. Struct. Mol. Biol.* **23**, 859–864 (2016).
 47. Grishaev, A., Yao, L., Ying, J., Pardi, A. & Bax, A. Chemical Shift Anisotropy of Imino ¹⁵N Nuclei in Watson - Crick Base Pairs from Magic Angle Spinning Liquid Crystal NMR and Nuclear Spin Relaxation. *J. Am. Chem. Soc.* **131**, 9490–9491 (2009).
 48. Dittmer, J., Kim, C.-H. & Bodenhausen, G. Similarities between intra- and intermolecular hydrogen bonds in RNA kissing complexes found by means of cross-correlated relaxation. *J. Biomol. NMR* **26**, 259–275 (2003).
 49. Dingley, A. J. & Grzesiek, S. Direct Observation of Hydrogen Bonds in Nucleic Acid Base Pairs by Internucleotide 2J_{HN} Couplings. *J. Am. Chem. Soc.* **7863**, 714–718 (1998).
 50. Wijmenga, S. S. & van Buuren, B. N. M. The use of NMR methods for conformational studies of nucleic acids. *Prog. Nucl. Magn. Reson. Spectrosc.* **32**, 287–387 (1998).
 51. Rinnenthal, J., Klinkert, B., Narberhaus, F. & Schwalbe, H. Direct observation of the temperature-induced melting process of the Salmonella fourU RNA thermometer at base-pair resolution. *Nucleic Acids Res.* **38**, 3834–47 (2010).
 52. Adrian, M., Heddi, B. & Phan, A. T. NMR spectroscopy of G-quadruplexes. *Methods* **57**, 11–24 (2012).
 53. Bhattacharya, P. K., Cha, J. & Barton, J. K. ¹H NMR determination of base-pair lifetimes in oligonucleotides containing single base mismatches. *Nucleic Acids Res.* **30**, 4740–4750 (2002).
 54. Dethoff, E. A., Petzold, K., Chugh, J., Casiano-negrone, A. & Al-Hashimi, H. M. Visualizing transient low-populated structures of RNA. *Nature* **491**, 724–728 (2012).
 55. Takeuchi, K., Arthanari, H. & Wagner, G. Perspective : revisiting the field dependence of TROSY sensitivity. *J. Biomol. NMR* **66**, 221–225 (2016).
 56. Czernek, J. An ab Initio Study of Hydrogen Bonding Effects on the Tensors in the Watson - Crick Base Pairs ¹⁵N and ¹H Chemical Shielding. *J. Phys. Chem.* **105**, 1357–1365 (2001).
 57. Shaka, A. J., Barker, P. B. & Freeman, R. Computer-optimized decoupling scheme for wideband applications and low-level operation. *J. Magn. Reson.* **64**, 547–552 (1985).
 58. Serganov, A., Yuan, Y., Pikovskaya, O., Polonskaia, A., Malinina, L., Phan, A. T., Hobartner, C., Micura, R., Breaker, R. R. & Patel, D. J. Structural Basis for Discriminative Regulation of Gene Expression by Adenine- and Guanine-Sensing mRNAs. *Chem. Biol.* **11**, 1729–1741 (2004).
 59. Ziegeler, M., Cevec, M., Richter, C. & Schwalbe, H. NMR Studies of HAR1 RNA Secondary Structures Reveal Conformational Dynamics in the Human RNA. *Chembiochem* **13**, 2100–2112 (2012).

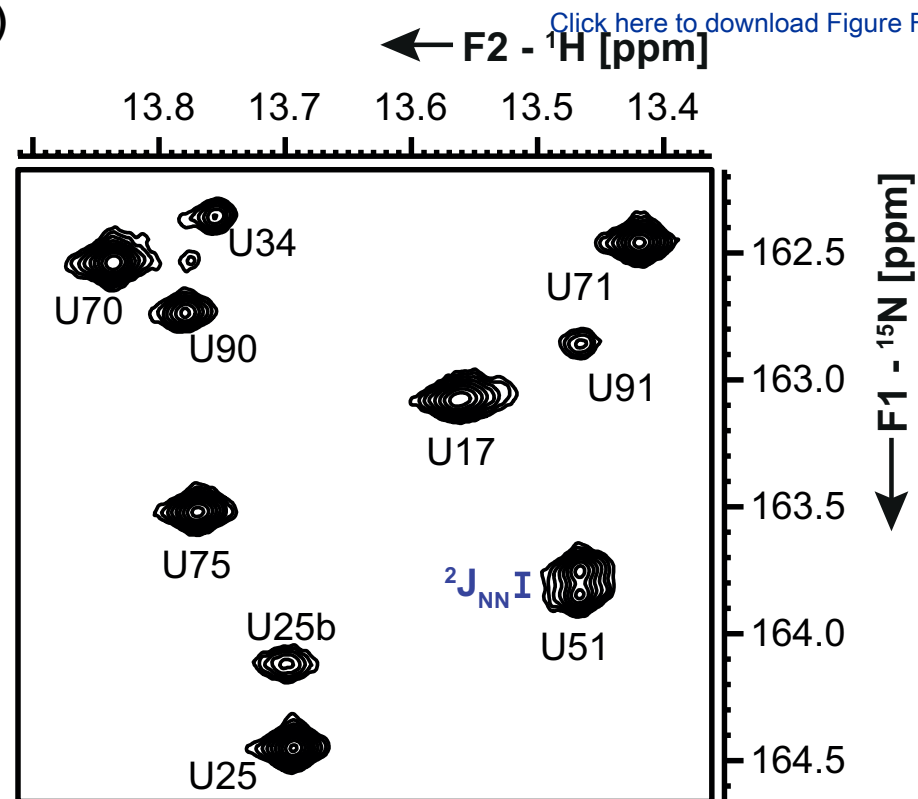




A)



B)



C)

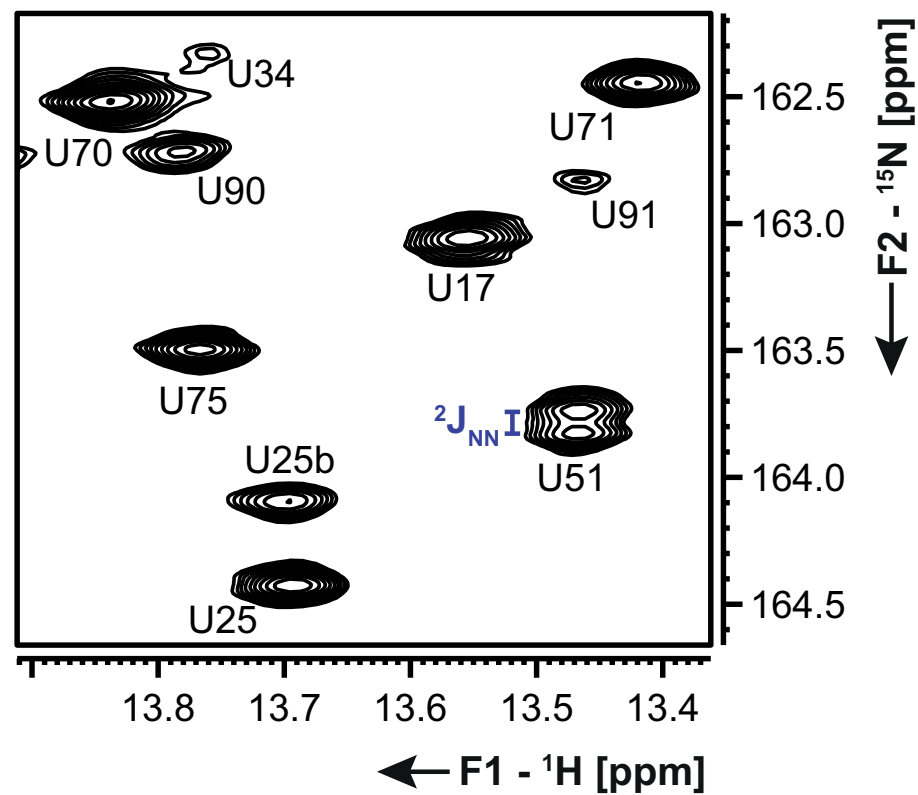
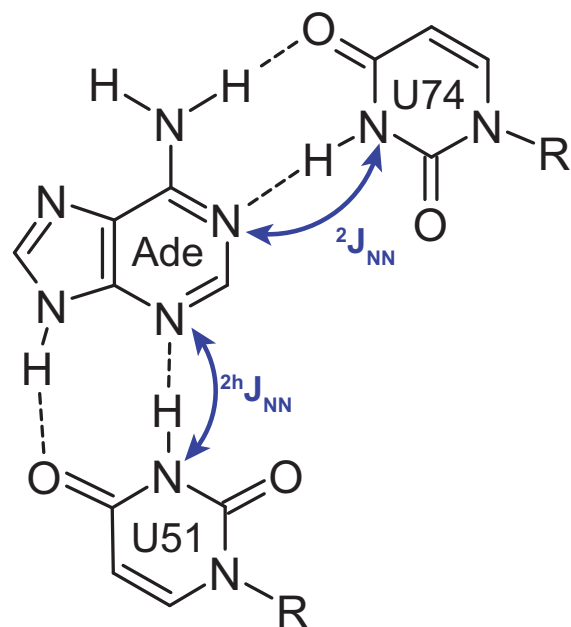
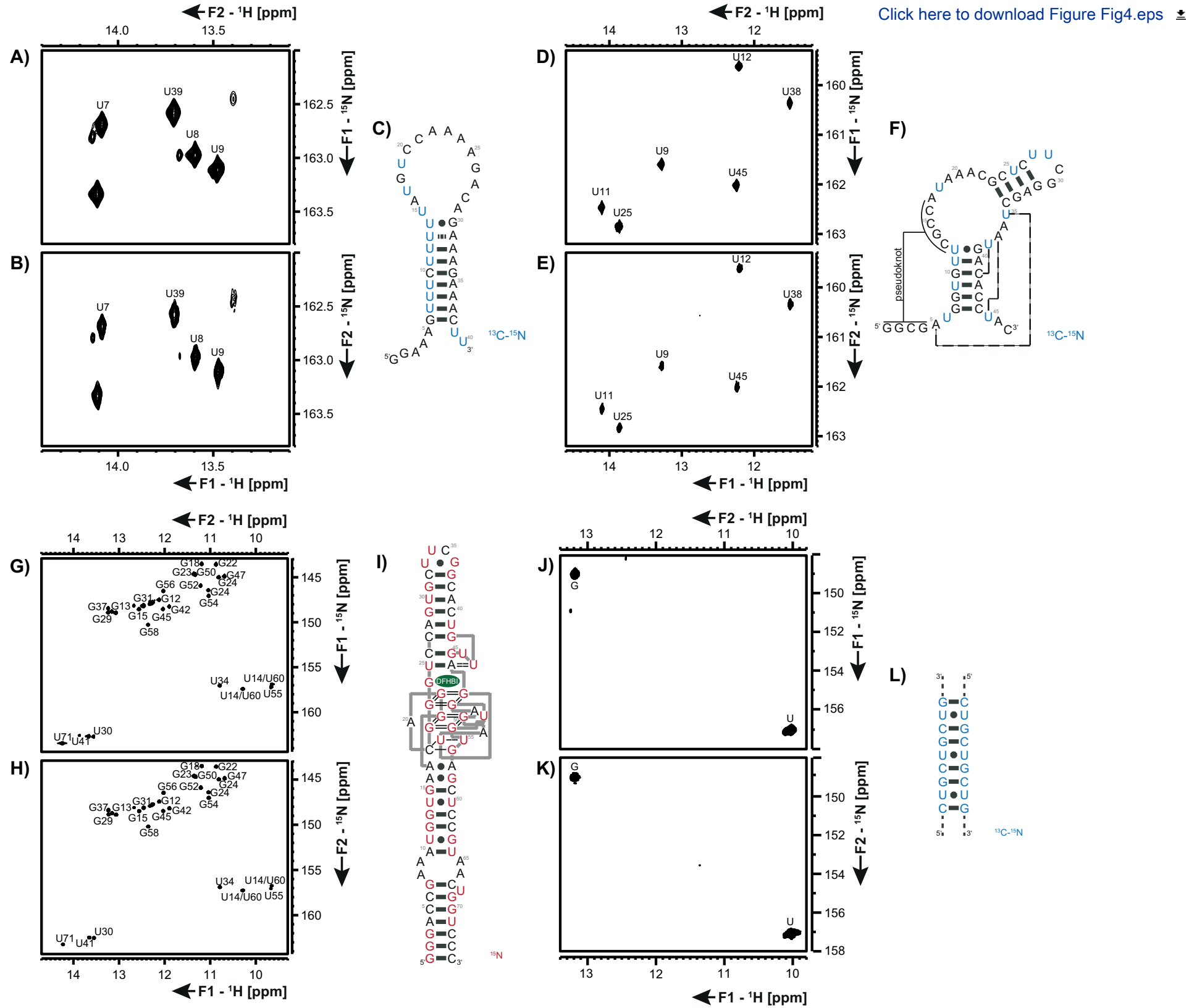
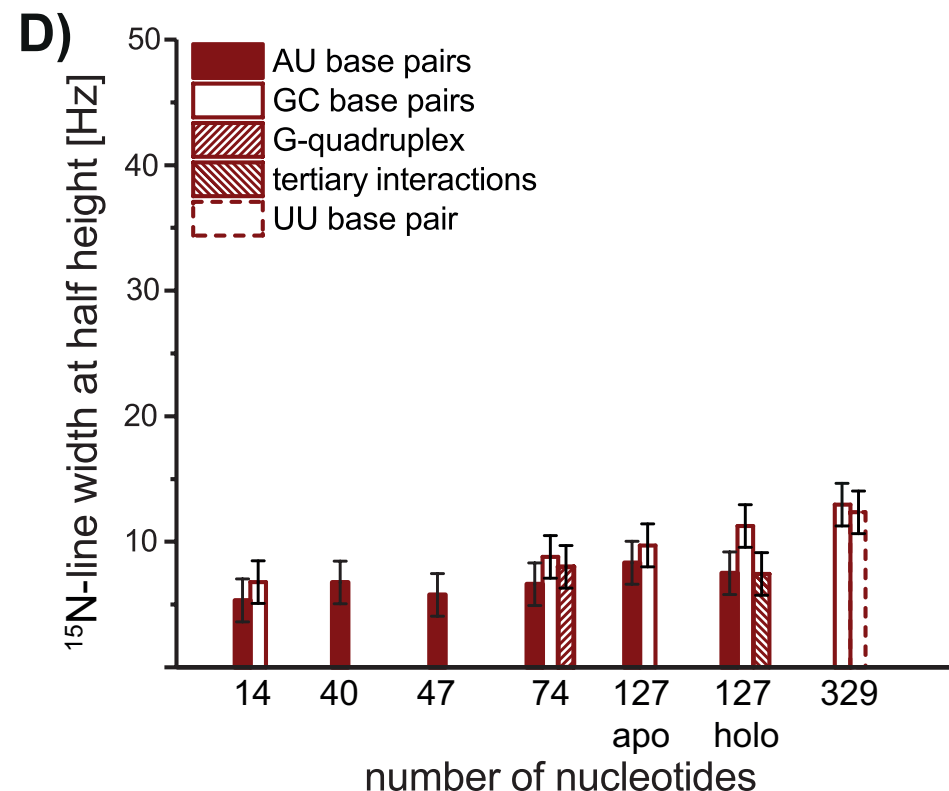
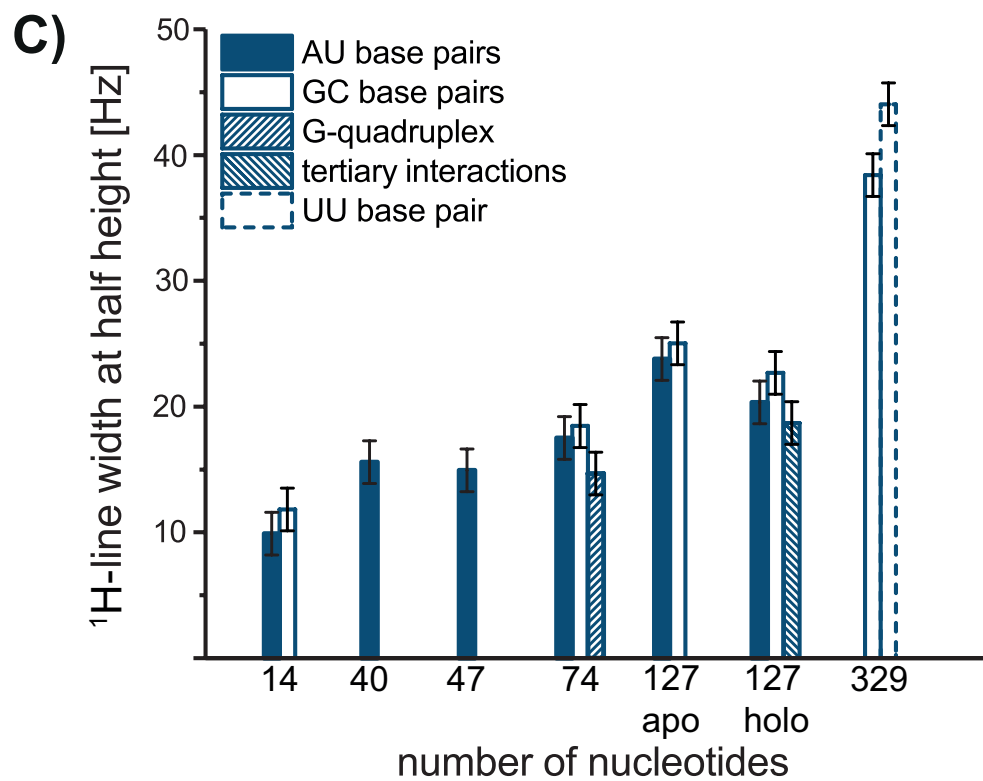
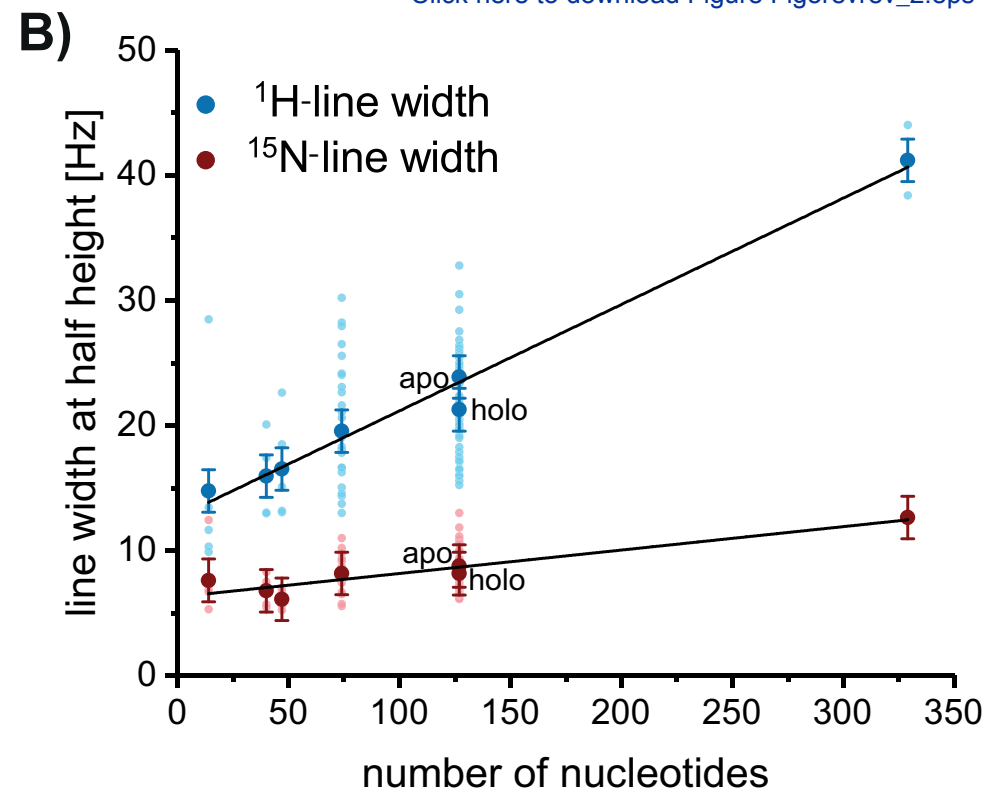
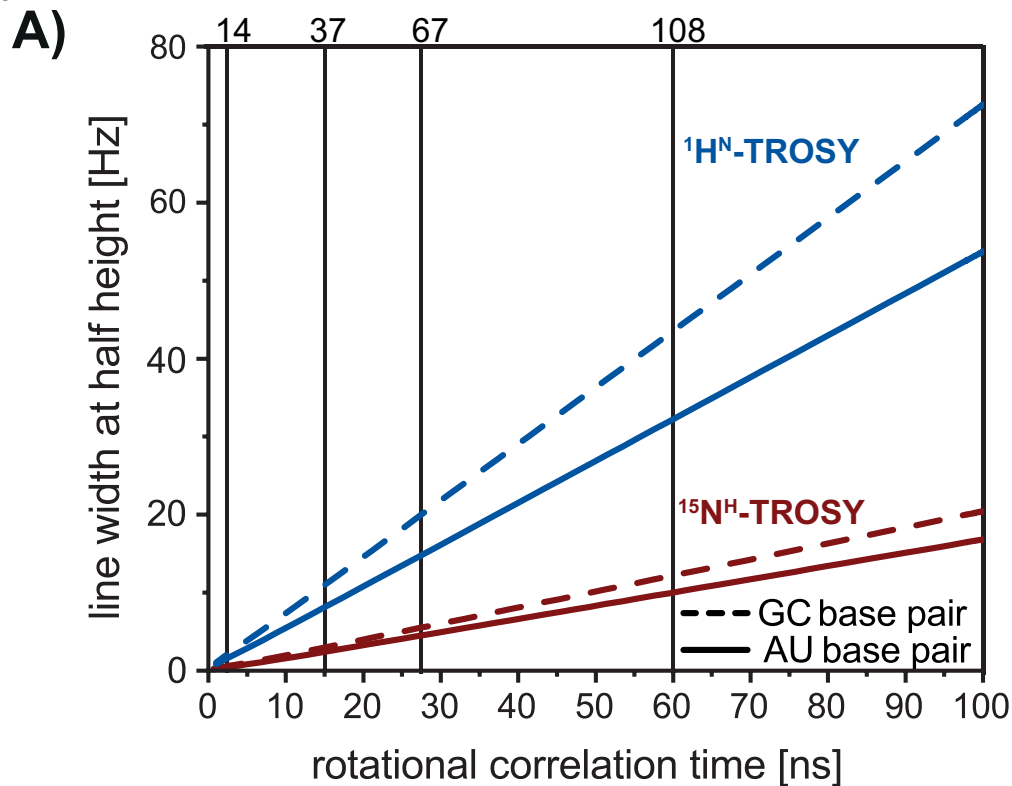
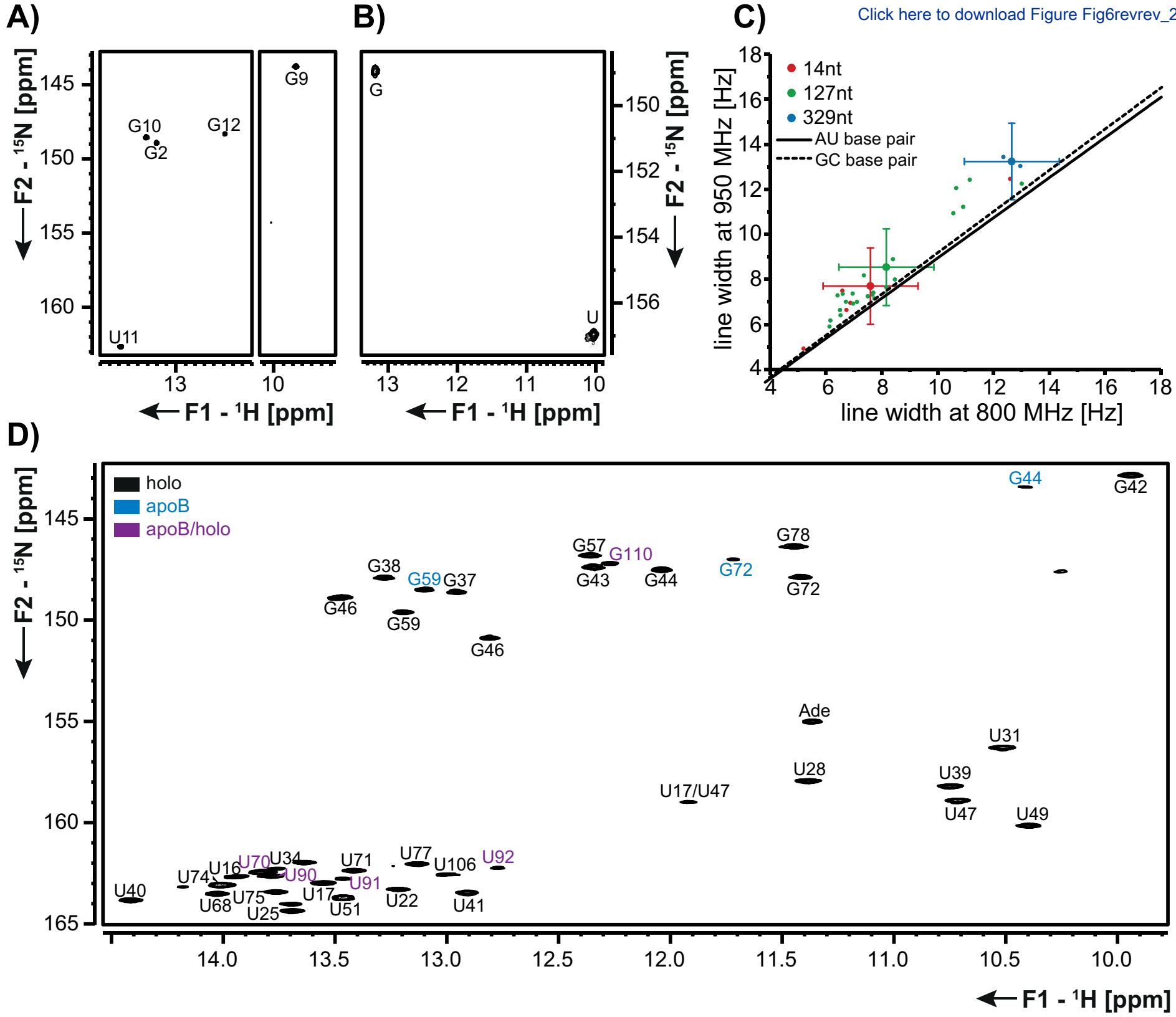


Figure 4







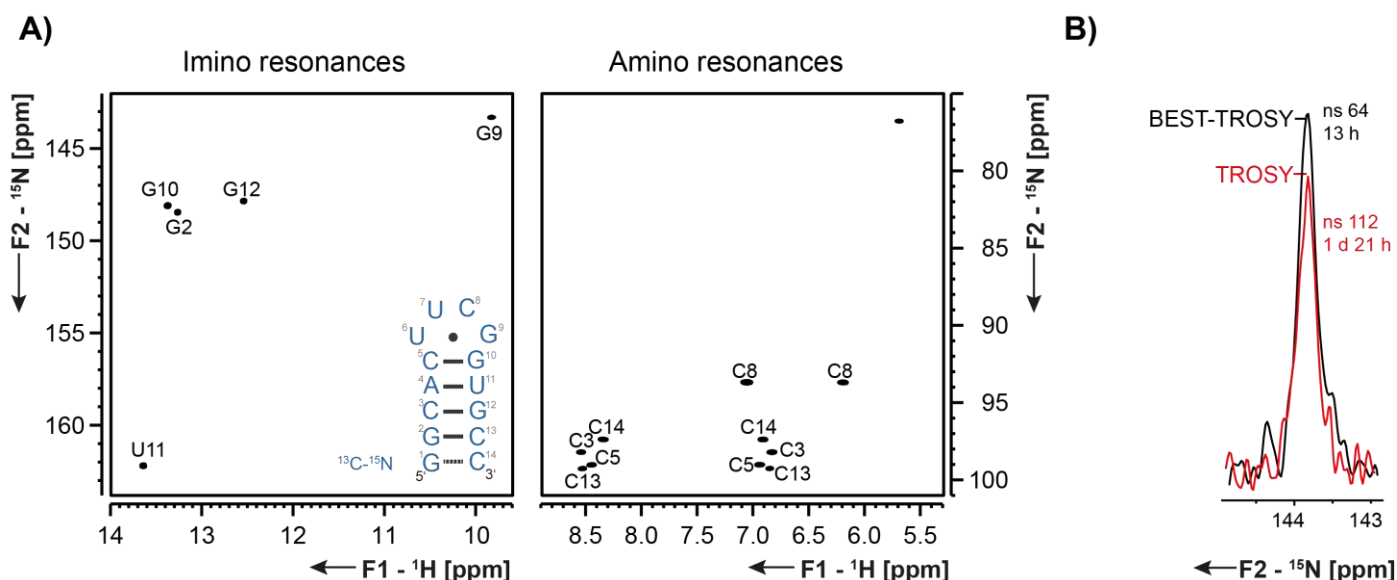
Supplementary Information

Evaluation of ^{15}N -detected H-N correlation experiments on increasingly large RNAs

Robbin Schnieders¹, Christian Richter¹, Sven Warhaut¹, Vanessa de Jesus¹, Sara Keyhani¹, Elke Duchardt-Ferner², Heiko Keller², Jens Wöhnert², Lars T. Kuhn³, Alexander L. Breeze³, Wolfgang Bermel⁴, Harald Schwalbe^{1,*}, Boris Fürtig^{1,*}

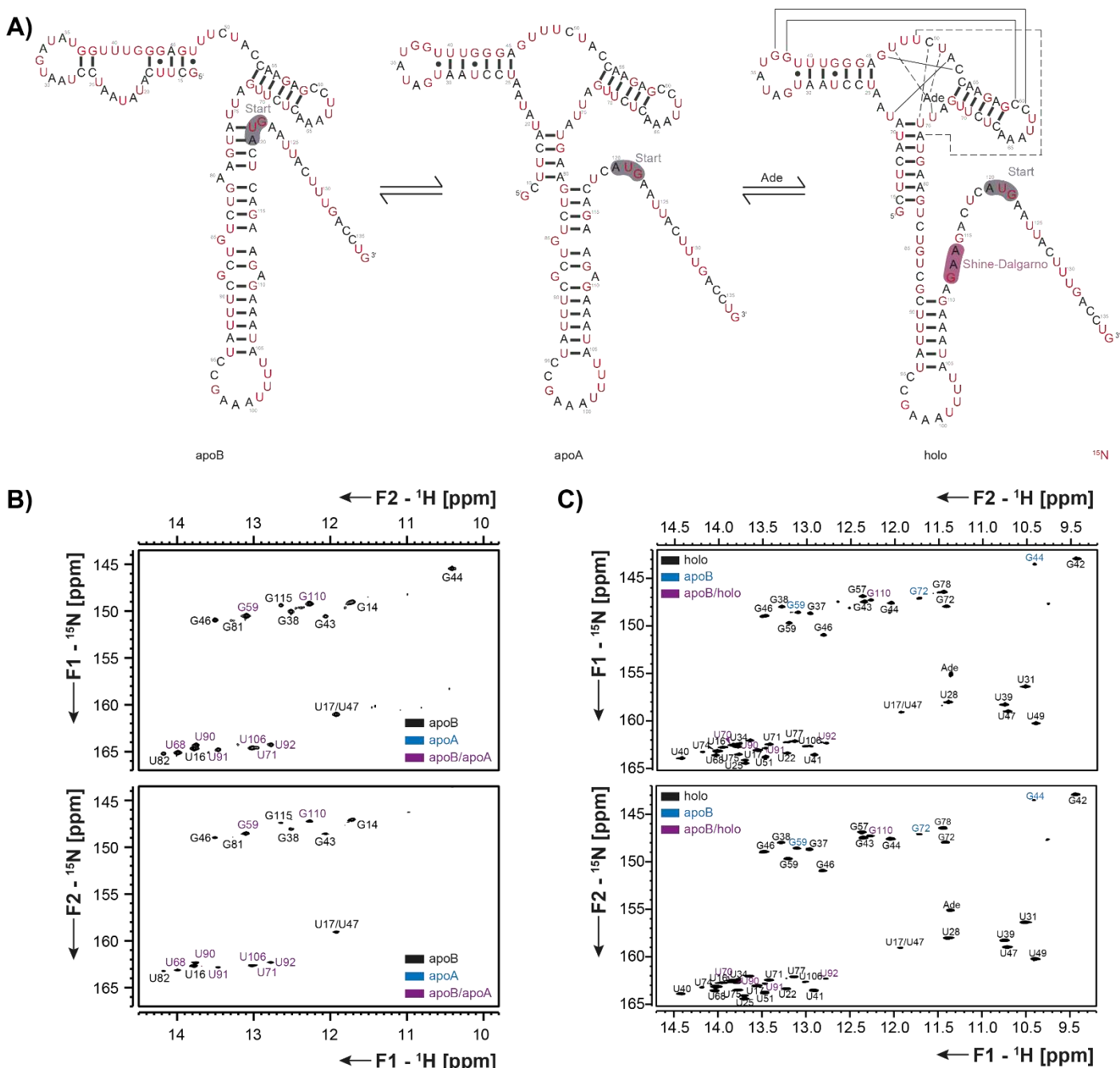
*correspondence to Prof. Dr. Harald Schwalbe – schwalbe@nmr.uni-frankfurt.de, 069 798 29737 or to Dr. Boris Fürtig – fuertig@nmr.uni-frankfurt.de, 069 798 29157

^{15}N detected H-N correlation experiments were applied to a 14 nt RNA with UUCG tetraloop¹. Besides TROSY and BEST-TROSY experiments (main text Fig 2), also a ^{15}N -detected HSQC-experiment was conducted (Suppl. Fig 1), which yielded less signal-to-noise per unit time in comparison with both of the TROSY experiments.



Suppl. Fig 1: A) 2D ^{15}N -detected HSQC spectra of the 14 nt RNA with UUCG tetraloop of the imino (left) and amino (right) region recorded on a 800 MHz NMR spectrometer equipped with a TXO-probe at 298 K. The spectrum of the imino region (left) was recorded with spectral widths of 35 ppm and 4.4 ppm in the direct ^{15}N - and indirect ^1H -dimension, respectively. The acquisition times were 0.3 s and 0.04 s, respectively. Carrier frequencies for ^{15}N , ^1H and ^{13}C were set to 155 ppm, 11.8 ppm and 150 ppm. Hard pulses were applied with field strength of 6.4 kHz (^{15}N), 17.5 kHz (^1H) and 21.9 kHz (^{13}C). Conducting 128 scans per increment with an inter-scan delay of 1 s resulted in an overall experimental time of 15 h. The spectrum with the amine resonances (right) was recorded with spectral widths of 32.6 ppm and 4.6 ppm in the direct ^{15}N - and indirect ^1H -dimension, respectively. 264 complex points were recorded in the ^{15}N - and 64 complex points in the ^1H -dimension while carrier frequencies were set to 86 ppm (^{15}N), 7.1 ppm (^1H) and 150 ppm (^{13}C). Hard pulses were applied with field strength of 6.9 kHz (^{15}N), 20.4 kHz (^1H) and 19.2 kHz (^{13}C). With 128 scans per increment and an inter-scan delay of 1 s an overall experimental time of 5 h resulted. **B)** Overlay of 1D rows for peak G9 for the ^{15}N -detected TROSY (red) and the ^{15}N -detected BEST-TROSY (black) experiments. Spectra were scaled to the same amplitude of noise.

Since the BEST-TROSY experiment yielded the best S/N ratio per unit time of the nitrogen direct detected experiments, it was recorded for six RNA constructs of different chain length and compared to a ^1H -detected BEST-TROSY experiment. The 127 nt riboswitch was investigated in the presence of its cognate ligand adenine and in the absence of ligand (Suppl. Fig 3 B and C).



Suppl. Fig 2: A) Secondary structures for all of the three states apoB, apoA and holo of the 127 nt adenine sensing riboswitch² with respective equilibrium pathways. ^{15}N labeled residues are colored in red. The spectra (B and C) were all recorded at 298 K at 800 MHz (18.8 T) NMR spectrometers, one equipped with a TCI probe for the ^1H -detected experiment and the other one equipped with a TXO probe for the nitrogen-detected TROSY experiment. **B)** ^1H - (top) and ^{15}N -detected (bottom) BEST-TROSY spectra of the 500 μM 127 nt riboswitch in the absence of ligand adenine. The ^1H -detected spectrum was recorded with spectral widths of 25 ppm in the direct ^1H - and 28 ppm in the indirect ^{15}N -dimension. Carrier frequencies for ^1H , ^{13}C and ^{15}N were set to 4.7 ppm, 101 ppm and 153 ppm, respectively. Hard pulses were applied with field strengths of 22.2 kHz (^1H), 22.3 kHz (^{13}C) and 7.6 kHz (^{15}N), respectively. Acquisition times were set to 0.3 s in the direct ^1H -dimension and to 0.06 s in the indirect ^{15}N -dimension. With 64 scans per increment and an inter-scan delay of 0.5 s the final measurement time was 4 h. The ^{15}N -detected spectrum was

recorded with spectral widths of 35 ppm in the direct ^{15}N - and 4.3 ppm in the indirect ^1H -dimension. Carrier frequencies for ^{15}N , ^{13}C and ^1H were set to 152.5 ppm, 150 ppm and 12.15 ppm, respectively. Hard pulses were applied with field strength of 7.3 kHz (^{15}N), and 20.4 kHz (^1H). Acquisition times were set to 0.3 s in the direct ^{15}N -dimension and 0.02 s in the indirect ^1H -dimension, respectively. GARP4 decoupling sequences on carbon nuclei were conducted with 1.8 kHz. With 368 scans per increment and a relaxation delay of 0.3 s the final measurement time was 23 h. **C)** ^1H - (top) and ^{15}N -detected (bottom) BEST-TROSY spectra of the 400 μM 127 nt riboswitch in the presence of 5 mM Mg^{2+} and 2 equivalents of adenine were recorded at 800 MHz at 298 K, respectively. Carrier frequencies for the ^1H -detected BEST-TROSY experiment were 4.7 ppm (^1H), 101 ppm (^{13}C) and 153 ppm (^{15}N) respectively. The spectral widths were chosen to be 25 ppm (^1H) and 28 ppm (^{15}N) respectively. Hard pulses on ^1H and ^{15}N were applied with field strengths of 21.7 kHz and 7.6 kHz respectively. The experiment was conducted with 64 number of scans and acquisition times of 0.3 s in the direct and 0.3 s in the indirect dimension. With a relaxation delay of 0.5 s resulted a total time for the experiment of 20 h 30 min. The ^{15}N detected BEST-TROSY experiment was recorded with carrier frequencies for ^{15}N , ^{13}C and ^1H of 155 ppm, 120 ppm and 12.175 ppm respectively. Spectral widths of 35 ppm in the direct and 5.2 ppm in the indirect dimension were covered. Hard pulses were carried out using field strength of 7.3 kHz (^{15}N) and 21.3 kHz (^1H). The number of scans per increment were set to 576 and the relaxation delay to 0.2 s. The experiment was recorded for 20 h with acquisition times of 0.3 s in the ^{15}N and 0.03 s in the ^1H -dimension.

Detailed parameters for spectra of Fig 4 in the main text:

A) ^1H -detected BEST-TROSY spectrum of a 2 mM uridine labeled 40 nt expression platform of the 2'-dG sensing riboswitch. It was recorded with a spectral width 4 ppm in the indirect ^{15}N dimension, while the carrier frequency for ^{15}N was set to 162 ppm. Hard ^1H pulses were applied with a field strength of 24.8 kHz. The acquisition time was 0.3 s in the indirect dimension. With 16 scans per increment and an inter-scan delay of 0.5 s the final measurement time was 1 h.

B) ^{15}N -detected BEST-TROSY spectrum of a 2 mM uridine labeled 40 nt expression platform of the 2'-dG sensing riboswitch. It was recorded with a spectral width 3.3 ppm in the indirect ^1H -dimension, while the corresponding carrier frequency was set to 13.8 ppm. Hard pulses were applied with field strength of 6.4 kHz (^{15}N), and 17.4 kHz (^1H). The acquisition time was 0.15 s in the indirect ^1H -dimension. With 16 scans per increment and an inter-scan delay of 0.3 s the final measurement time was 2.5 h.

D) ^1H -detected BEST-TROSY spectrum of a 1 mM ^{13}C - ^{15}N uridine labeled 47 nt fluoride riboswitch. It was recorded with a spectral width of 4.5 ppm in the indirect ^{15}N -dimension, while the corresponding carrier frequency was set to 161.25 ppm. Hard ^1H pulses were applied with a field strength of 25.6 kHz and the acquisition time was set to 0.3 s in the indirect dimension. With 16 scans per increment and an inter-scan delay of 0.4 s the final measurement time was 1 h.

E) ^{15}N -detected BEST-TROSY spectrum of a 1 mM ^{13}C - ^{15}N uridine labeled 47 nt fluoride riboswitch. It was recorded with a spectral width 2.8 ppm in the indirect ^1H -dimension, while the corresponding carrier frequency was set to 12.5 ppm. Hard pulses were applied with field strength of 7.0 kHz (^{15}N), and 18.5 kHz (^1H). The acquisition time was 0.15 s in the indirect ^1H -dimension. With 32 scans per increment and an inter-scan delay of 0.3 s the final measurement time was 4.5 h.

G) ^1H -detected BEST-TROSY spectrum of a 200 μM ^{15}N uridine and guanosine labeled 74 nt Spinach RNA. It was recorded with a spectral width 22 ppm in the indirect ^{15}N -dimension, while the corresponding carrier frequency was set to 153.5 ppm. Hard ^1H pulses were applied with field strength of 24.7 kHz and the

acquisition time in the indirect dimension was set to 0.3 s. With 32 scans per increment and an inter-scan delay of 0.4 s the final measurement time was 10 h.

H) ¹⁵N-detected BEST-TROSY spectrum of a 200 μM ¹⁵N uridine and guanosine labeled 74 nt Spinach RNA. It was recorded with a spectral width of 5.3 ppm in the indirect ¹H-dimension, while the corresponding carrier frequency was set to 11.95 ppm. Hard pulses were applied with field strength of 7.0 kHz (¹⁵N), and 20.8 kHz (¹H). The acquisition time was set 0.15 s in the indirect ¹H-dimension. With 128 scans per increment and an inter-scan delay of 0.3 s the final measurement time was 33 h.

J) ¹H-detected BEST-TROSY spectrum of a 700 μM ¹³C-¹⁵N labeled 329 nt CUG repeat RNA. It was recorded with a spectral width 11.4 ppm in the indirect ¹⁵N-dimension, while the corresponding carrier frequency was set to 153 ppm. Hard ¹H pulses were applied with a field strength of 22.3 kHz. The acquisition time was set to 0.07 s in the indirect ¹⁵N-dimension. With 48 scans per increment and an inter-scan delay of 0.5 s the final measurement time was 1.5 h.

K) ¹⁵N-detected BEST-TROSY spectrum of a 700 μM ¹³C-¹⁵N labeled 329 nt CUG repeat RNA. It was recorded with a spectral width of 4.15 ppm in the indirect ¹H-dimension, while the corresponding carrier frequency was set to 11.6 ppm. Hard pulses were applied with field strength of 7.3 kHz (¹⁵N), and 20.3 kHz (¹H). The acquisition time was 0.03 s in the indirect ¹H-dimension. With 64 scans per increment and an inter-scan delay of 0.2 s the final measurement time was 20 h.

Simulations of relaxation rates

Relaxation rates were simulated using equations for transverse relaxation in TROSY-experiments (1-12). Some of the parameters used for predicting the relaxation rates differ for GC and AU base pairs (Suppl. Suppl. Table 1), which results in a different relaxation behavior (Fig 4 main text) for the Watson-Crick type base pairs. Further ¹H^N-¹H distances were measured for GC and AU base pairs, respectively from the structure of the 14 nt RNA with UUCG tetraloop (2KOC)¹ for U11-H3 and G12-H3 (5'-pppG¹G²C³A⁴C⁵U⁶U⁷C⁸G⁹G¹⁰U¹¹G¹²C¹³C¹⁴-3'). Those differences in distances lead to proton-proton relaxation contributions to the dipole-dipole relaxation. Distances were as follows: U11: 2.2 Å, 3.8 Å, 2.9 Å, 4.2 Å, 4.8 Å, 3.9 Å, 4.5 Å, 4.6 Å, 4.5 Å, 4.9 Å and G12: 2.2 Å, 2.4 Å, 3.9 Å, 3.5 Å, 4.9 Å, 4.7 Å, 4.8 Å, 4.9 Å, 4.5 Å, 3.8 Å, 4.1 Å. Relaxation rates were calculated for a magnetic field strength of 18.8 T corresponding to an 800 MHz NMR spectrometer.

$$R_{2H}^{TROSY} = R_{2H}^{dip} + R_{2H}^{csa} + R_{2H}^{HH} - R_{2H}^{int} \quad (1)$$

$$R_{2N}^{TROSY} = R_{2N}^{dip} + R_{2N}^{csa} + R_{1N}^{HH} - R_{2N}^{int} \quad (2)$$

$$R_{2I}^{dip} = \frac{P_{IS}^2}{8} [4J(0) + 3J(\omega_I) + J(|\omega_I - \omega_S|) + 3J(\omega_I) + 6J(\omega_I + \omega_S)] \quad (3)$$

R_{2I}^{dip} = transverse relaxation of spin I due to dipolar interactions, $J(\omega)$ = spectral density, ω_{IS} = Larmor frequency of spins I/S

$$R_{2I}^{csa} = \frac{\delta_I^2}{6} [4J(0) + 3J(\omega_I)] + \frac{\delta_S^2}{2} J(\omega_S) \quad (4)$$

R_{2I}^{csa} = transverse relaxation of spin I due to chemical shift anisotropy

(5)

$$R_{2H}^{HH} = \frac{p_{HH}^2}{8} [5J(0) + 9J(\omega_H) + 6J(2\omega_H)]$$

R_{2HH} = transverse relaxation of H due to remote protons

$$R_{1N}^{HH} = \frac{p_{HH}^2}{8} [J(0) + 3J(\omega_H) + 6J(2\omega_H)] \quad (6)$$

R_{1HH} = relaxation of N due to remote protons

$$R_{2I}^{int} = \frac{C p_{IS} \delta_I [4J(0) + 3J(\omega_I)]}{\sqrt{8} \cdot \sqrt{6}} \quad (7)$$

R_{2int} = relaxation due to cross correlation of CSA and dipole-dipole interactions

$$p_{IS} = \left(\frac{\mu_0}{4\pi} \right) \frac{\gamma_I \gamma_S \hbar}{r_{IS}^3} \quad (8)$$

p_{IS} = dipole-dipole relaxation, μ_0 = vacuum permeability, γ_I = gyromagnetic ratio of spin I, γ_S = gyromagnetic ratio of spin S, \hbar = planck constant divided by 2π , r_{IS} = distance between spins I and S

$$p_{HH} = \left(\frac{\mu_0}{4\pi} \right) \frac{\gamma_H \gamma_H \hbar}{r_{HH}^3} \quad (9)$$

$$J(\omega) = \frac{2\tau_C}{5(1 + (\tau_C \omega)^2)} \quad (10)$$

τ_C = rotational correlation time, ω = spectrometer frequency

$$\delta_I = \left(\frac{1}{\sqrt{3}} \right) \gamma_I B_0 \Delta\sigma_I \quad (11)$$

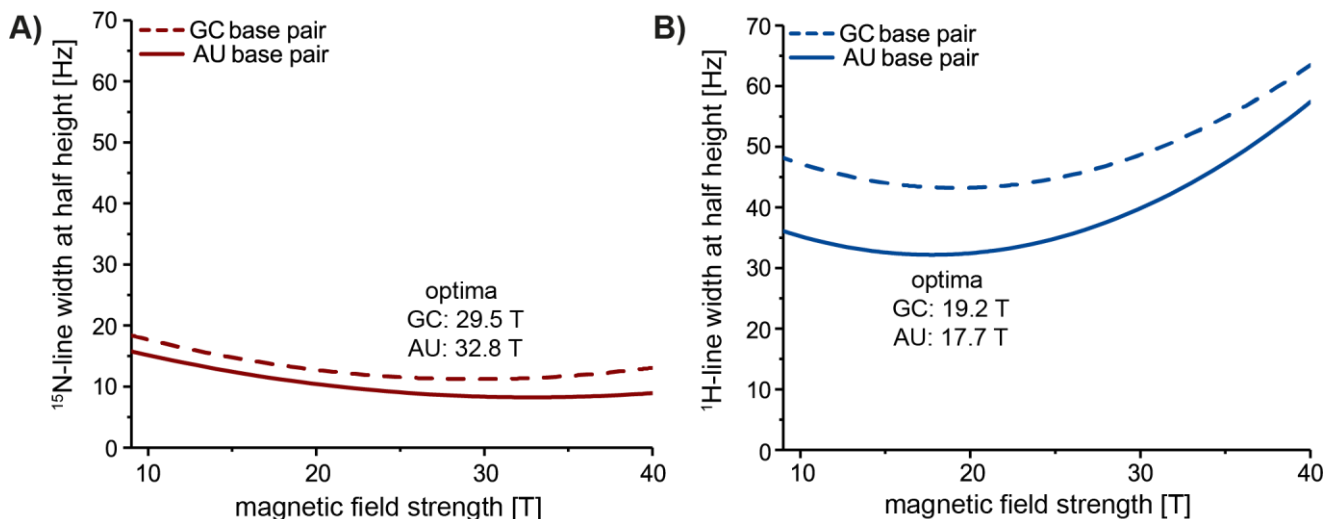
δ_I = relaxation caused by CSA, B_0 = magnetic field strength, $\Delta\sigma_I$ = chemical shift anisotropy

$$C = (3 \cos^2 \theta - 1) \quad (12)$$

C = angular dependence of cross correlation, θ = angle between the tensor axis of dipole-dipole and CSA interactions

Suppl. Table 1: Overview of parameters for GC and AU base pairs, respectively.

	GC base pair	AU base pair
$\Delta\sigma_N^3$	-116.85 ppm	-102.75 ppm
$\Delta\sigma_H^4$	19.65 ppm	20.45 ppm
r_{NH}^3	1.043 Å	1.057 Å
θ_N^3	13.1°	11.4°
θ_H^5	1.9°	2.3°



Suppl. Fig 5: Simulation of the ^{15}N -line width for AU (blue) and GC (red) base pairs in dependence of the magnetic field strength using equations 1-12. The field strength optima are marked, respectively. Simulations have been conducted with a rotational correlation time of 60 ns.

References

1. Nozinovic, S., Fürtig, B., Jonker, H. R. A., Richter, C. & Schwalbe, H. High-resolution NMR structure of an RNA model system: the 14-mer cUUCGg tetraloop hairpin RNA. *Nucleic Acids Res.* **38**, 683–94 (2010).
2. Reining, A., Nozinovic, S., Schlepckow, K., Buhr, F., Fürtig, B. & Schwalbe, H. Three-state mechanism couples ligand and temperature sensing in riboswitches. *Nature* **499**, 355–9 (2013).
3. Grishaev, A., Yao, L., Ying, J., Pardi, A. & Bax, A. Chemical Shift Anisotropy of Imino ^{15}N Nuclei in Watson - Crick Base Pairs from Magic Angle Spinning Liquid Crystal NMR and Nuclear Spin Relaxation. *J. Am. Chem. Soc.* **131**, 9490–9491 (2009).
4. Dittmer, J., Kim, C.-H. & Bodenhausen, G. Similarities between intra- and intermolecular hydrogen bonds in RNA kissing complexes found by means of cross-correlated relaxation. *J. Biomol. NMR* **26**, 259–275 (2003).
5. Czernek, J. An ab Initio Study of Hydrogen Bonding Effects on the Tensors in the Watson - Crick Base Pairs ^{15}N and ^1H Chemical Shielding. *J. Phys. Chem.* **105**, 1357–1365 (2001).